Hygrothermoelastic analysis of multilayered composite and sandwich shells

(Article begins on next page)

04 August 2020

Hygrothermoelastic analysis of multilayered composite and sandwich shells

S. Brischetto*

Abstract

Refined two-dimensional models are proposed for the static hygrothermoleastic analysis of multilayered composite and sandwich shells. These shell models are developed in the framework of the Carrera's Unified Formulation (in a general and unified manner) by considering both equivalent single layer and layer wise multilayer description. The Principle of Virtual Displacements contains elastic, thermal and hygroscopic strains. The governing equations allow mechanical, thermal and hygroscopic loads to be applied and they are solved in a closed form solution. Thermal and hygroscopic loads are defined by means of appropriate temperature and moisture content profiles through the thickness of the shell, such profiles can "a priori" be assumed or they can be calculated by solving the Fourier heat conduction equation and the Fick moisture diffusion law. Such equations are solved in steady-state conditions and in curvilinear coordinates for the shell geometries. The presence of loads due to hygroscopic and thermal effects (in addition to the mechanical load) modifies the bending response of multilayered shells. Comparisons between classical and refined models, and between assumed and calculated temperature and moisture content profiles are proposed in the cases of composite and sandwich shells. The use of refined models combined with calculated temperature and moisture content profiles through the thickness is mandatory for a correct elasto-thermo-hygroscopic analysis of multilayered structures.

Keywords: multilayered shells, composite layers, sandwich configurations, refined shell models, classical shell models, hygrothermal loads, Fourier equation of heat conduction, Fick law for the mass transport of the moisture content.

1 Introduction

Aircraft structures can be modelled via shell models which are effective element schemes applicable to both membrane-dominated and bending-dominated behaviors. Such structures are often exposed to high temperature and humidity environmental conditions. In particular, the introduction of composite and sandwich shells has increased the negative effects concerning the moisture absorbtion under adverse operating conditions [1]. The hygrothermal effects give a degradation of mechanical properties of the material and they also generate both hygroscopic and thermal loads which get worse the bending response of multilayered shells. The present work is mainly focused on the second investigation type in analogy with the plate case already seen in Brischetto and Carrera [2]. Moisture and temperature expansion have the same magnitude and moisture penetrates into the material by "Fickian" diffusion

---
*Corresponding author: Salvatore Brischetto, Assistant Professor, Department of Mechanical and Aerospace Engineering, Politecnico di Torino, Corso Duca degli Abruzzi 24, 10129 Torino, ITALY. tel: +39.011.090.6813, fax: +39.011.090.6899, e.mail: salvatore.brischetto@polito.it.

which takes place if [3], [4]: - heat transfer through the material is only by conduction (use of the Fourier law); - the moisture diffusion is described by the Fick law; - the temperature approaches equilibrium much faster than the moisture concentration which means decoupled energy (Fourier) and mass transfer (Fick) equations; - the thermal conductivity and mass diffusivity depend only on temperature. A further simplification, with respect to "Fickian" diffusion, made in this work is that thermal conductivity and moisture diffusion coefficients do not depend on the temperature. The analogy between heat conduction and moisture diffusion, as suggested in [5], is very powerful in the analysis of hygrothermal effects for the bending problem of multilayered shells. Such an analogy has preliminary been discussed in [6] and [7] and the Fick second law of diffusion has experimentally been validated in [8]. In the present work the Fourier heat conduction equation has been solved using the methodology proposed in [9], both plate and shell geometries have been considered in [10]-[12]. The Fick diffusion law will be solved in analogy with the methodology already proposed for the Fourier equation, such a method has been detailed for plate geometry in [2] and it will be extended to shell structures in this work by using geometrical interfaces. In some cases the use of a linear temperature and/or moisture content profile through the thickness could be enough depending on the shell thickness ratio and lamination sequence.

Considerable work has been done to understand the effects of hygrothermal environment on the mechanical behavior of composite plates, a deep review of the main research activities in this field has been given in [2] and [13]. A brief review of the most important works about the hygrothermal effects in multilayered shells is given in the following, they concern the static and bending analysis, the failure and damage investigation, the free vibrations and dynamic analysis and the buckling and post-buckling behavior. Naidu and Sinha [14] have used a finite element formulation to investigate the large deflection bending behavior of composite cylindrical shell panels subjected to hygrothermal environments. Wuthrich [15] has analyzed the effects of hygrothermal expansion in the stress analysis of long thick-walled composite tubes subjected to internal and external pressure, longitudinal forces and twisting moments. An exact elasticity solution has been obtained in [16] for the stresses and displacements in an orthotropic cylindrical shell loaded by an external pressure under imposed constant moisture concentrations on the inner and outer surfaces. The three-dimensional stress analysis proposed in [17] has been applied to a fiber-reinforced organic matrix composite cylindrical segment subjected to hygrothermal and mechanical loads which may vary radially and circumferentially, but not axially. Effects of moisture and temperature on the behavior of composite T-joints made of carbon fibre composite materials have been investigated in [18], the analysis has been carried out by using a modified thick shell element that takes into account the hygrothermal effects. Lal et alii [19] have investigated the effect of random system properties on transverse nonlinear central deflection of laminated composite spherical shell panel subjected to hygro-thermo-mechanical loading, the higher order shear deformation theory and von-Karman nonlinear kinematics have been used for basic mathematical formulation. Nosier and Miri [20] have studied free-edge effects in laminated, circular, cylindrical shell panels subjected to hygrothermal loading, a combination of equivalent single layer and layer wise shell theories has been used. A general stress analysis has been developed in [21] for thick and thin multi-layered composite cylinders under hygrothermal loadings, uniform and parabolic temperature distributions have been chosen for the thermal loads and analytical solutions have been compared with the finite element solutions. A hygrothermal model for analyzing composite laminates under both mechanical and hygrothermal loadings has been constructed by the variational asymptotic method in [22] where the results have been compared with the exact hygrothermal solutions, classical lamination theory and first-order shear-deformation theory in order to assess the capability of the method proposed. Hygrothermal cycles are known to cause degradation of composite materials due to moisture uptake and thermal expansion. The knowledge of internal stresses due to cyclic environmental conditions is necessary to forecast a possible damage occurrence in the material during its service life. In [23], a self-consistent model has been used in order to predict the stress state at the microscopic scale (fiber and matrix) induced by the real and accelerated cycles. Ghosh [24] has investigated the initiation and

progress of damage in laminated composite shells at elevated moisture concentration and temperature due to low velocity impacts via a FE analysis. Free vibrations and dynamic analysis are also important for shell investigation in hygrothermal environment, a quadratic isoparametric finite element formulation based on the first order shear deformation theory has been presented in [25] for the free vibration and transient response analysis of multiple doubly curved composite shells subjected to hygrothermal environment. Dynamic responses of an orthotropic plate subjected to hygrothermal environments have been optimized in [26], the geometry has been discretized into specially developed 3D shell composite elements which are able to handle hygrothermal effects of our own design. The dynamic behavior of a stiffened composite laminated conical thin shell under hygrothermal loads has been studied numerically in [27], the governing equations of truncated conical shell have been based on the Donnell-Mushtari theory of thin shells including the transverse shear deformation and rotary inertia, the effects of moisture has been examined in the dynamic behavior. Raja et alii [28] have proposed the active stiffening and active compensation analyses to present the influence of active stiffness on the dynamic behavior of piezo-hygro-thermo-elastic laminates. A coupled piezoelectric finite element formulation involving a hygrothermal strain field has been derived using the virtual work principle and it has been employed in a nine-node field consistent Lagrangian element. Buckling and post-buckling behavior of multilayered shells has a dependence from the hygrothermal environment as demonstrated in the following works. Kundu and Han [29] have investigated the vibration characteristics of pre- and post-buckled hygro-thermo-elastic laminated composite doubly curved shells, in fact, due to the change in environmental conditions, hygrothermal residual stresses may induce buckling and dynamic instability in composite shell structures. The effects of hygrothermal conditions on the buckling and post-buckling of laminated cylindrical shells have been investigated in [30] where the results have showed that the hygrothermal environment has a significant effect. Huang [31] has investigated the viscoelastic buckling and post-buckling of fibre reinforced cylindrical shells in hygrothermal environment when subjected to an external pressure. A quasi-elastic finite element approach has been employed for the structural response. Hygrothermal stresses due to the change in environmental condition may induce buckling and dynamic instability in the composite shell structures. In [32], the hygrothermoelastic buckling behavior of laminated composite shells has been numerically simulated using geometrically nonlinear finite element method. The effect of random system properties on the post buckling load of geometrically nonlinear laminated composite cylindrical shell panel subjected to hygrothermomechanical loading has been investigated in [33] where the higher order shear deformation theory and von-Karman nonlinear kinematics have been used for the basic formulation. Shen [34], [35] has investigated the effect of hygrothermal conditions on the buckling and post-buckling of laminated cylindrical panels subjected to axial compression using a micro-to-macro-mechanical analytical model, the governing equations are based on Reddy's higher order shear deformation shell theory [34] and on classical lamination theory [35] with von Karman-Donnell-type of kinematic nonlinearity. An investigation has been carried out in [36] and [37] to understand hydrothermal effects on locally delaminated buckling near the surface of a cylindrical laminated shell. The effect of non-linear buckling for local delamination of cylindrical laminated shells has been obtained by considering transverse displacements of the sub-laminated shell.

The present paper proposes the static analysis of cylindrical shell panels subjected to a transverse pressure applied at the top, the hygrothermal effects are evaluated in terms of displacements and stresses. The constitutive and geometrical relations consider the elastic, thermal and hygroscopic contributions as suggested in Sections 2 and 3. Displacement vector, temperature and moisture content are approximated in two-dimensional form by means of the Carrera's Unified Formulation (CUF) [38] which allows classical and refined shell models to be obtained (see Section 4). The Principle of Virtual Displacements (PVD) for elasto-thermo-hygroscopic problems is given in Section 5 and governing equations are solved in a closed form solution where mechanical, hygroscopic and thermal loads can be applied. In thermal and hygroscopic loads the temperature and moisture content profiles through the thickness of the shell can a priori be assumed or can be calculated by solving the Fourier heat conduc-

3

tion equation and the Fick moisture diffusion law, respectively. Section 6 gives several results about multilayered composite and sandwich shells. Such benchmarks are proposed after some preliminary assessments (where mechanical [39], thermal [40] and hygroscopic [13] loads are separately applied) given to validate the refined CUF models. The main conclusions are discussed in Section 7.

2 Constitutive equations

In the elasto-thermo-hygroscopic analysis of multilayered shells the strain components $\boldsymbol{\epsilon}$ are given as an algebraic summation of the elastic part $\boldsymbol{\epsilon}_u$, the thermal part $\boldsymbol{\epsilon}_\theta$ and the hygroscopic contribution $\boldsymbol{\epsilon}_\mathcal{M}$ for each k layer [1]-[3]:

$$\boldsymbol{\epsilon}^k = (\epsilon_{\alpha\alpha}^k \ \epsilon_{\beta\beta}^k \ \epsilon_{zz}^k \ \gamma_{\beta z}^k \ \gamma_{\alpha z}^k \ \gamma_{\alpha\beta}^k)^T = \boldsymbol{\epsilon}_u^k + \boldsymbol{\epsilon}_\theta^k + \boldsymbol{\epsilon}_\mathcal{M}^k \,, \tag{1}$$

the elastic contribution (subscript u) is defined by means of the geometrical relations for shells as it will be detailed in the Section 3. The superscript T means transpose of a vector. (α,β,z) are the curvilinear coordinates of the shell geometry (see Figure 1). The thermal strain contribution (subscript θ) is due to the scalar over-temperature $\theta = (T_1 - T_0)$ (T_1 means applied temperature and T_0 is the room external reference temperature):

$$\boldsymbol{\epsilon}_\theta^k = (\epsilon_{\alpha\alpha\theta}^k \ \epsilon_{\beta\beta\theta}^k \ \epsilon_{zz\theta}^k \ \gamma_{\beta z\theta}^k \ \gamma_{\alpha z\theta}^k \ \gamma_{\alpha\beta\theta}^k)^T = -\boldsymbol{\alpha}^k \ \theta^k \,, \tag{2}$$

where the thermal expansion coefficients are grouped in a vector of 6×1 dimension for each k layer:

$$\boldsymbol{\alpha}^k = (\alpha_{11}^k \ \alpha_{22}^k \ \alpha_{33}^k \ 0 \ 0 \ \alpha_{12}^k)^T \,. \tag{3}$$

The hygroscopic strain terms (subscript $\mathcal{M}$) are due to the scalar moisture content $\mathcal{M}$:

$$\boldsymbol{\epsilon}_\mathcal{M}^k = (\epsilon_{\alpha\alpha\mathcal{M}}^k \ \epsilon_{\beta\beta\mathcal{M}}^k \ \epsilon_{zz\mathcal{M}}^k \ \gamma_{\beta z\mathcal{M}}^k \ \gamma_{\alpha z\mathcal{M}}^k \ \gamma_{\alpha\beta\mathcal{M}}^k)^T = -\boldsymbol{\beta}^k \ \mathcal{M}^k \,, \tag{4}$$

the moisture content $\mathcal{M}$ in non-dimensional form (or in percentage %) is defined by means of the following ratio:

$$\mathcal{M} = \frac{W - W_d}{W_d} \times (100) = \frac{W_d + W_c - W_d}{W_d} \times (100) = \frac{W_c}{W_d} \times (100) \,, \tag{5}$$

where $W = W_d + W_c$ is the mass of moist material, W_c is the total mass of the moisture in the material and W_d is the mass of dry material. The total mass of the moisture in the material is the integral in the volume V of the moisture concentration c given in $[kg/m^3]$:

$$W_c = \int_V c \, dV \,, \tag{6}$$

the mass of dry material is the integral in the volume V of the mass density of the dry material ρ_d given in $[kg/m^3]$:

$$W_d = \int_V \rho_d \, dV \,. \tag{7}$$

Eqs.(6) and (7) can be introduced in Eq.(5):

$$\mathcal{M} = \frac{c \, V}{\rho_d \, V} \times (100) = \frac{c}{\rho_d} \times (100) \,, \tag{8}$$

the moisture content $\mathcal{M}$ is non-dimensional form and it can also be given in percentage % if it is multiplied by 100. The moisture concentration c is in $[kg/m^3]$ and it gives the moisture content $\mathcal{M}$

when it is divided by the mass density of the dry material ρ_d. Further details about the moisture content $\mathcal{M}$ can be found in [2]. The moisture expansion coefficients are grouped in a vector of 6×1 dimension for each k layer:

$$\boldsymbol{\beta}^k = (\beta_{11}^k \ \beta_{22}^k \ \beta_{33}^k \ 0 \ 0 \ \beta_{12}^k)^T . \tag{9}$$

The over-temperature θ is in $[K]$ and the relative thermal expansion coefficients α_{ij} are in $[\frac{1}{K}]$. The moisture content $\mathcal{M}$ is in non-dimensional form $[-]$ and the relative moisture expansion coefficients β_{ij} are in non-dimensional form $[-]$ too. The moisture content $\mathcal{M}$ can also be given in percentage $\%$, in this case the relative expansion coefficients β_{ij} are given as $[\frac{1}{\%}]$. Eqs.(2) and (4) are substituted in Eq.(1) in order to obtain the general form of the strain components for the elasto-thermo-hygroscopic analysis:

$$\boldsymbol{\epsilon}^k = \boldsymbol{\epsilon}_u^k - \boldsymbol{\alpha}^k \ \theta^k - \boldsymbol{\beta}^k \ \mathcal{M}^k . \tag{10}$$

The Hooke law written in the problem reference system (α, β, z) of the shell is [4]:

$$\boldsymbol{\sigma}^k = \boldsymbol{Q}^k \ \boldsymbol{\epsilon}^k , \tag{11}$$

the strain $\boldsymbol{\epsilon}^k$ has the form given in Eq.(10), the vector of elasto-thermo-hygroscopic stress components is $\boldsymbol{\sigma}^k = (\sigma_{\alpha\alpha}^k \ \sigma_{\beta\beta}^k \ \sigma_{zz}^k \ \sigma_{\beta z}^k \ \sigma_{\alpha z}^k \ \sigma_{\alpha\beta}^k)^T$ and the matrix of the elastic coefficients $\boldsymbol{Q}^k$ has 6×6 dimension:

$$\boldsymbol{Q}^k = \begin{bmatrix} Q_{11}^k & Q_{12}^k & Q_{13}^k & 0 & 0 & Q_{16}^k \\ Q_{12}^k & Q_{22}^k & Q_{23}^k & 0 & 0 & Q_{26}^k \\ Q_{13}^k & Q_{23}^k & Q_{33}^k & 0 & 0 & Q_{36}^k \\ 0 & 0 & 0 & Q_{44}^k & Q_{45}^k & 0 \\ 0 & 0 & 0 & Q_{45}^k & Q_{55}^k & 0 \\ Q_{16}^k & Q_{26}^k & Q_{36}^k & 0 & 0 & Q_{66}^k \end{bmatrix} . \tag{12}$$

The stress components $\boldsymbol{\sigma}$ are the summation of the elastic part $\boldsymbol{\sigma}_u$, the thermal part $\boldsymbol{\sigma}_\theta$ and the hygroscopic contribution $\boldsymbol{\sigma}_\mathcal{M}$ for each k layer [1], [3]:

$$\boldsymbol{\sigma}^k = \boldsymbol{\sigma}_u^k + \boldsymbol{\sigma}_\theta^k + \boldsymbol{\sigma}_\mathcal{M}^k . \tag{13}$$

The constitutive equation for the elasto-thermo-hygroscopic analysis is (use of Eqs.(2), (4), (10), (11) and (13)):

$$\boldsymbol{\sigma}^k = \boldsymbol{\sigma}_u^k + \boldsymbol{\sigma}_\theta^k + \boldsymbol{\sigma}_\mathcal{M}^k = \boldsymbol{Q}^k \ \boldsymbol{\epsilon}_u^k - \boldsymbol{\lambda}^k \ \theta^k - \boldsymbol{\mu}^k \ \mathcal{M}^k , \tag{14}$$

the first term in Eq.(14) is the classical Hooke law for the pure elastic problem. The vector $\boldsymbol{\lambda}^k$ contains the thermo-mechanical coupling coefficients and has 6×1 dimension:

$$\boldsymbol{\lambda}^k = \boldsymbol{Q}^k \ \boldsymbol{\alpha}^k = (\lambda_{11}^k \ \lambda_{22}^k \ \lambda_{33}^k \ 0 \ 0 \ \lambda_{12}^k)^T , \tag{15}$$

the vector $\boldsymbol{\mu}^k$ contains the hygroscopic-mechanical coupling coefficients and has 6×1 dimension:

$$\boldsymbol{\mu}^k = \boldsymbol{Q}^k \ \boldsymbol{\beta}^k = (\mu_{11}^k \ \mu_{22}^k \ \mu_{33}^k \ 0 \ 0 \ \mu_{12}^k)^T . \tag{16}$$

The constitutive equation will be included in the Principal of Virtual Displacements in order to obtain the relative governing equations after the integration by parts. This integration by parts is made easier if the equations proposed will be split in in-plane (p) and out-of-plane (n) components. The Eq.(14) is split as:

$$\boldsymbol{\sigma}_p^k = \boldsymbol{\sigma}_{pu}^k + \boldsymbol{\sigma}_{p\theta}^k + \boldsymbol{\sigma}_{p\mathcal{M}}^k = \boldsymbol{Q}_{pp}^k \ \boldsymbol{\epsilon}_{pu}^k + \boldsymbol{Q}_{pn}^k \ \boldsymbol{\epsilon}_{nu}^k - \boldsymbol{\lambda}_p^k \ \theta^k - \boldsymbol{\mu}_p^k \ \mathcal{M}^k , \tag{17}$$

$$\boldsymbol{\sigma}_n^k = \boldsymbol{\sigma}_{nu}^k + \boldsymbol{\sigma}_{n\theta}^k + \boldsymbol{\sigma}_{n\mathcal{M}}^k = \boldsymbol{Q}_{np}^k \ \boldsymbol{\epsilon}_{pu}^k + \boldsymbol{Q}_{nn}^k \ \boldsymbol{\epsilon}_{nu}^k - \boldsymbol{\lambda}_n^k \ \theta^k - \boldsymbol{\mu}_n^k \ \mathcal{M}^k , \tag{18}$$

where the stress and strain components are:

$$\boldsymbol{\sigma}_p^k = (\sigma_{\alpha\alpha}^k \ \sigma_{\beta\beta}^k \ \sigma_{\alpha\beta}^k)^T, \qquad \boldsymbol{\sigma}_n^k = (\sigma_{\alpha z}^k \ \sigma_{\beta z}^k \ \sigma_{zz}^k)^T, \tag{19}$$

$$\boldsymbol{\epsilon}_p^k = (\epsilon_{\alpha\alpha}^k \ \epsilon_{\beta\beta}^k \ \gamma_{\alpha\beta}^k)^T, \qquad \boldsymbol{\epsilon}_n^k = (\gamma_{\alpha z}^k \ \gamma_{\beta z}^k \ \epsilon_{zz}^k)^T, \tag{20}$$

the split procedure given in Eqs.(19) and (20) is also valid for the elastic (subscript u), thermal (subscript θ) and hygroscopic (subscript $\mathcal{M}$) components of stress and strain vectors. The matrix of elastic coefficients in Eq.(12) is split in four sub-arrays of 3×3 dimension:

$$\boldsymbol{Q}_{pp}^k = \begin{bmatrix} Q_{11} & Q_{12} & Q_{16} \\ Q_{12} & Q_{22} & Q_{26} \\ Q_{16} & Q_{26} & Q_{66} \end{bmatrix}^k, \quad \boldsymbol{Q}_{pn}^k = \begin{bmatrix} 0 & 0 & Q_{13} \\ 0 & 0 & Q_{23} \\ 0 & 0 & Q_{36} \end{bmatrix}^k, \tag{21}$$

$$\boldsymbol{Q}_{np}^k = \begin{bmatrix} 0 & 0 & 0 \\ 0 & 0 & 0 \\ Q_{13} & Q_{23} & Q_{36} \end{bmatrix}^k, \quad \boldsymbol{Q}_{nn}^k = \begin{bmatrix} Q_{55} & Q_{45} & 0 \\ Q_{45} & Q_{44} & 0 \\ 0 & 0 & Q_{33} \end{bmatrix}^k.$$

The vectors of thermo-mechanical coupling coefficients (Eq.(15)) and hygroscopic-mechanical coupling coefficients (Eq.(16)) are split as:

$$\boldsymbol{\lambda}_p^k = \begin{bmatrix} \lambda_{11} \\ \lambda_{22} \\ \lambda_{12} \end{bmatrix}^k, \quad \boldsymbol{\lambda}_n^k = \begin{bmatrix} 0 \\ 0 \\ \lambda_{33} \end{bmatrix}^k, \quad \boldsymbol{\mu}_p^k = \begin{bmatrix} \mu_{11} \\ \mu_{22} \\ \mu_{12} \end{bmatrix}^k, \quad \boldsymbol{\mu}_n^k = \begin{bmatrix} 0 \\ 0 \\ \mu_{33} \end{bmatrix}^k. \tag{22}$$

3   Geometrical relations

The elastic contribution (subscript u) in Eq.(1) is defined by means of the geometrical relations which have the following matrix form for the shell geometry:

$$\boldsymbol{\epsilon}_u^k = (\epsilon_{\alpha\alpha u}^k \ \epsilon_{\beta\beta u}^k \ \epsilon_{zzu}^k \ \gamma_{\beta zu}^k \ \gamma_{\alpha zu}^k \ \gamma_{\alpha\beta u}^k)^T = (\boldsymbol{D}^k + \boldsymbol{A}^k) \, \boldsymbol{u}^k, \tag{23}$$

where the displacement vector $\boldsymbol{u}^k = (u^k \ v^k \ w^k)^T$ has three components in the three directions α, β and z (see Figure 1). The matrix $\boldsymbol{D}$ contains the differential operators and it has dimension 6×3 and the matrix $\boldsymbol{A}$ (dimension 6×3) contains the pure geometrical contributions:

$$\boldsymbol{D}^k = \begin{bmatrix} \frac{\partial_\alpha}{H_\alpha^k} & 0 & 0 \\ 0 & \frac{\partial_\beta}{H_\beta^k} & 0 \\ 0 & 0 & \partial_z \\ 0 & \partial_z & \frac{\partial_\beta}{H_\beta^k} \\ \partial_z & 0 & \frac{\partial_\alpha}{H_\alpha^k} \\ \frac{\partial_\beta}{H_\beta^k} & \frac{\partial_\alpha}{H_\alpha^k} & 0 \end{bmatrix}, \quad \boldsymbol{A}^k = \begin{bmatrix} 0 & 0 & \frac{1}{H_\alpha^k R_\alpha^k} \\ 0 & 0 & \frac{1}{H_\beta^k R_\beta^k} \\ 0 & 0 & 0 \\ 0 & -\frac{1}{H_\beta^k R_\beta^k} & 0 \\ -\frac{1}{H_\alpha^k R_\alpha^k} & 0 & 0 \\ 0 & 0 & 0 \end{bmatrix}, \tag{24}$$

where the partial derivatives mean $\partial_\alpha = \frac{\partial}{\partial\alpha}$, $\partial_\beta = \frac{\partial}{\partial\beta}$ and $\partial_z = \frac{\partial}{\partial z}$. The metric coefficients H_α^k, H_β^k and H_z^k are $\sqrt{g_1}$, $\sqrt{g_2}$ and $\sqrt{g_3}$, respectively, where g_1, g_2 and g_3 are:

$$g_1 = (1 + \frac{z_k}{R_\alpha^k})^2, \quad g_2 = (1 + \frac{z_k}{R_\beta^k})^2, \quad g_3 = 1. \tag{25}$$

The radii of curvature R_α^k and R_β^k are clearly indicated in Figure 1. Details about shell geometry and the relative geometrical equations can be found in [41] where the square of an infinitesimal linear segment in the layer, the associated infinitesimal area and volume are given by:

$$ds_k^2 = H_\alpha^{k\,2}\, d\alpha_k^2 \; + \; H_\beta^{k\,2}\, d\beta_k^2 + H_z^{k\,2}\, dz_k^2 \; , \tag{26}$$

$$d\Omega_k = H_\alpha^k H_\beta^k\, d\alpha_k\, d\beta_k \; , \tag{27}$$

$$dV_k = H_\alpha^k\, H_\beta^k\, H_z^k\, d\alpha_k\, d\beta_k\, dz_k \; , \tag{28}$$

where the metric coefficients also depend on the k layer and on the z thickness coordinate.

The geometrical relations will also be included in the Principal of Virtual Displacements in order to obtain the governing equations. These last will be proposed in a closed form which means that an integration by parts will be performed. This integration by parts is made easier if the equations proposed will be split in in-plane (p) and out-of-plane (n) components:

$$\epsilon_{pu}^k = (\epsilon_{\alpha\alpha u}^k\; \epsilon_{\beta\beta u}^k\; \gamma_{\alpha\beta u}^k)^T = (\boldsymbol{D}_p^k + \boldsymbol{A}_p^k)\; \boldsymbol{u}^k \; , \tag{29}$$

$$\epsilon_{nu}^k = (\gamma_{\alpha z u}^k\; \gamma_{\beta z u}^k\; \epsilon_{zz u}^k)^T = (\boldsymbol{D}_{np}^k + \boldsymbol{D}_{nz}^k - \boldsymbol{A}_n^k)\; \boldsymbol{u}^k \; , \tag{30}$$

the explicit form of the introduced arrays follows:

$$\boldsymbol{D}_p^k = \begin{bmatrix} \frac{\partial_\alpha}{H_\alpha^k} & 0 & 0 \\ 0 & \frac{\partial_\beta}{H_\beta^k} & 0 \\ \frac{\partial_\beta}{H_\beta^k} & \frac{\partial_\alpha}{H_\alpha^k} & 0 \end{bmatrix} \; , \quad \boldsymbol{D}_{np}^k = \begin{bmatrix} 0 & 0 & \frac{\partial_\alpha}{H_\alpha^k} \\ 0 & 0 & \frac{\partial_\beta}{H_\beta^k} \\ 0 & 0 & 0 \end{bmatrix} \; , \quad \boldsymbol{D}_{nz}^k = \begin{bmatrix} \partial_z & 0 & 0 \\ 0 & \partial_z & 0 \\ 0 & 0 & \partial_z \end{bmatrix} \; , \tag{31}$$

$$\boldsymbol{A}_p^k = \begin{bmatrix} 0 & 0 & \frac{1}{H_\alpha^k R_\alpha^k} \\ 0 & 0 & \frac{1}{H_\beta^k R_\beta^k} \\ 0 & 0 & 0 \end{bmatrix} \; , \boldsymbol{A}_n^k = \begin{bmatrix} \frac{1}{H_\alpha^k R_\alpha^k} & 0 & 0 \\ 0 & \frac{1}{H_\beta^k R_\beta^k} & 0 \\ 0 & 0 & 0 \end{bmatrix} \; . \tag{32}$$

4   Refined two-dimensional models

The application of a two-dimensional method for shells allows the unknown variables to be expressed as a set of thickness functions depending only on the thickness coordinate z and the correspondent variable depending on the in-plane curvilinear coordinates α and β. So that, the generic variable $\boldsymbol{a}(\alpha, \beta, z)$ and its variation $\delta\boldsymbol{a}(\alpha, \beta, z)$ are written according to the following general expansion:

$$\boldsymbol{a}^k(\alpha, \beta, z) = F_s(z)\boldsymbol{a}_s^k(\alpha, \beta) \; , \qquad \delta\boldsymbol{a}^k(\alpha, \beta, z) = F_\tau(z)\delta\boldsymbol{a}_\tau^k(\alpha, \beta) \; , \tag{33}$$
$$with \quad \tau, s = 1, \dots, N \; .$$

The function $\boldsymbol{a}$ could be the displacement vector $\boldsymbol{u}$, the scalar over-temperature θ or the scalar moisture content $\mathcal{M}$. Refined two-dimensional shell models are obtained by means of the Carrera's Unified Formulation (CUF) given in Eq.(33). CUF permits to obtain, in a general and unified manner, several models that can differ in the chosen order of expansion in the thickness direction and in the Equivalent Single Layer (ESL) or Layer Wise (LW) multilayer approach [10], [11], [12]. (α, β) are the in-plane coordinates and z the thickness one. The summing convention with repeated indexes τ and s is assumed. The order of expansion N goes from first to higher order values, and depending on the used thickness functions, a model can be ESL when the variable is assumed for the whole multilayer and a Taylor expansion is employed as thickness functions $F(z)$ (in this case the expansion does not depend on the k layer) or LW when the variable is separately considered in each layer and a combination of Legendre

polynomials are used as thickness functions $F(z)$ (in this case the expansion depends on the k layer). In CUF the maximum order of expansion N in z direction is the fourth.

The choice made in this work is that the displacement $\boldsymbol{u}$ can be approximated as ESL or LW through the thickness, while the over-temperature θ and the moisture content $\mathcal{M}$ are always given in LW form with the same order of expansion used for the displacements:

$$\boldsymbol{u}^k(\alpha, \beta, z) = F_s(z)\boldsymbol{u}_s^k(\alpha, \beta) = F_0 \boldsymbol{u}_0^k + F_1 \boldsymbol{u}_1^k + \ldots + F_N \boldsymbol{u}_N^k\,, \tag{34}$$

$$\theta^k(\alpha, \beta, z) = F_s(z)\theta_s^k(\alpha, \beta) = F_0 \theta_0^k + F_1 \theta_1^k + \ldots + F_N \theta_N^k\,, \tag{35}$$

$$\mathcal{M}^k(\alpha, \beta, z) = F_s(z)\mathcal{M}_s^k(\alpha, \beta) = F_0 \mathcal{M}_0^k + F_1 \mathcal{M}_1^k + \ldots + F_N \mathcal{M}_N^k\,, \tag{36}$$

when the displacement is given in ESL form the expansion in Eq.(34) does not depend on the k index.

A refined model is defined ESL or LW depending on the choice made for the displacement vector, in fact over-temperature and moisture content are always in LW form. ESL models are indicated with acronyms from ED1 to ED4 where E means ESL approach, D indicates the use of the PVD and the digit indicates the order of expansion N through the thickness. LW models are indicated with acronyms from LD1 to LD4 where L means LW approach.

First order Shear Deformation Theory (FSDT) [4] can be obtained as particular case of the ED1 model by imposing a constant transverse displacement w through the thickness direction. Classical Lamination Theory (CLT) [4] can be obtained from FSDT by imposing in the Hooke law an infinite transverse shear rigidity which means zero transverse shear strains $\gamma_{\alpha z}$ and $\gamma_{\beta z}$. Further details about CUF refined models can be found in [10], [11] and [12].

5 Principle of Virtual Displacements

For a generic volume V of the shell, the general form of the Principal of Virtual Displacements (PVD) is:

$$\int_V \left(\delta \boldsymbol{\epsilon}_{pu}^T \boldsymbol{\sigma}_p + \delta \boldsymbol{\epsilon}_{nu}^T \boldsymbol{\sigma}_n\right) dV = \delta L_e - \delta L_{in}\,, \tag{37}$$

where δL_e and δL_{in} are the external and inertial virtual works, respectively. $\delta \boldsymbol{\epsilon}_{pu}$ and $\delta \boldsymbol{\epsilon}_{nu}$ are the virtual elastic strains, and $\boldsymbol{\sigma}_p$ and $\boldsymbol{\sigma}_n$ are in-plane and out-of-plane elasto-thermo-hygroscopic stress components.

By considering a multilayered shell made of N_l layers, and the integral on the volume V_k of each k layer as an integral on the in plane domain Ω_k plus the integral in the thickness-direction domain A_k, it is possible to write the PVD for the static case as:

$$\sum_{k=1}^{N_l} \int_{\Omega_k} \int_{A_k} \left(\delta \boldsymbol{\epsilon}_{pu}^{kT} \boldsymbol{\sigma}_p^k + \delta \boldsymbol{\epsilon}_{nu}^{kT} \boldsymbol{\sigma}_n^k\right) d\Omega_k dz = \sum_{k=1}^{N_l} \delta L_e^k\,, \tag{38}$$

the elasto-thermo-hygroscopic stresses given by the Eqs.(17) and (18) can be introduced in Eq.(38):

$$\sum_{k=1}^{N_l} \int_{\Omega_k} \int_{A_k} \left(\delta \boldsymbol{\epsilon}_{pu}^{kT}(\boldsymbol{\sigma}_{pu}^k + \boldsymbol{\sigma}_{p\theta}^k + \boldsymbol{\sigma}_{p\mathcal{M}}^k) + \delta \boldsymbol{\epsilon}_{nu}^{kT}(\boldsymbol{\sigma}_{nu}^k + \boldsymbol{\sigma}_{n\theta}^k + \boldsymbol{\sigma}_{n\mathcal{M}}^k)\right) d\Omega_k dz = \sum_{k=1}^{N_l} \delta L_e^k\,. \tag{39}$$

Geometrical relations (Eqs.(29) and (30)), constitutive equations (Eqs.(17) and (18)) and CUF for displacements $\boldsymbol{u}^k$, over-temperature θ^k and moisture content $\mathcal{M}^k$ as described in Eqs.(34)-(36) can be

8

substituted in the PVD developed in Eqs.(38) and (39):

$$
\sum_{k=1}^{N_l} \int_{\Omega_k} \int_{A_k} \left(\left((\boldsymbol{D}_p^k + \boldsymbol{A}_p^k) F_\tau \delta \boldsymbol{u}_\tau^k \right)^T \left(\boldsymbol{Q}_{pp}^k (\boldsymbol{D}_p^k + \boldsymbol{A}_p^k) F_s \boldsymbol{u}_s^k + \boldsymbol{Q}_{pn}^k (\boldsymbol{D}_{np}^k + \boldsymbol{D}_{nz}^k - \boldsymbol{A}_n^k) F_s \boldsymbol{u}_s^k - \boldsymbol{\lambda}_p^k F_s \theta_s^k \right. \right. \quad (40)
$$

$$
\left. - \boldsymbol{\mu}_p^k F_s \mathcal{M}_s^k \right) + \left(\left((\boldsymbol{D}_{np}^k + \boldsymbol{D}_{nz}^k - \boldsymbol{A}_n^k) F_\tau \delta \boldsymbol{u}_\tau^k \right)^T \left(\boldsymbol{Q}_{np}^k (\boldsymbol{D}_p^k + \boldsymbol{A}_p^k) F_s \boldsymbol{u}_s^k + \boldsymbol{Q}_{nn}^k (\boldsymbol{D}_{np}^k + \boldsymbol{D}_{nz}^k - \boldsymbol{A}_n^k) F_s \boldsymbol{u}_s^k \right. \right.
$$

$$
\left. \left. - \boldsymbol{\lambda}_n^k F_s \theta_s^k - \boldsymbol{\mu}_n^k F_s \mathcal{M}_s^k \right) \right) d\Omega_k dz = \sum_{k=1}^{N_l} \delta L_e^k .
$$

In the case of shell geometries, it is important to remember the Eq.(27) for the integration domain $d\Omega_k$.

5.1 Governing equations

In order to obtain a strong form of differential equations on the domain Ω_k and the relative boundary conditions on edge Γ_k, the integration by parts is used in Eq.(40), it allows the differential operator to be moved from the infinitesimal variation of the generic displacement $\delta \boldsymbol{u}^k$ to the finite quantity $\boldsymbol{u}^k$ [10]-[12]. For a generic displacement $\boldsymbol{u}^k$, the integration by parts states:

$$
\int_{\Omega_k} \left(\boldsymbol{D}_\Omega^k \delta \boldsymbol{u}^k \right)^T \boldsymbol{u}^k d\Omega_k = - \int_{\Omega_k} \delta \boldsymbol{u}^{kT} \left(\boldsymbol{D}_\Omega^{kT} \boldsymbol{u}^k \right) d\Omega_k + \int_{\Gamma_k} \delta \boldsymbol{u}^{kT} \left(\boldsymbol{I}_\Omega^{kT} \boldsymbol{u}^k \right) d\Gamma_k , \quad (41)
$$

where $\Omega = p, np$. The matrices to perform the integration by parts have the following form, in analogy with matrices for the geometrical relations in Eqs.(31):

$$
\boldsymbol{I}_p^k = \begin{bmatrix} \frac{1}{H_\alpha^k} & 0 & 0 \\ 0 & \frac{1}{H_\beta^k} & 0 \\ \frac{1}{H_\beta^k} & \frac{1}{H_\alpha^k} & 0 \end{bmatrix} , \quad \boldsymbol{I}_{np}^k = \begin{bmatrix} 0 & 0 & \frac{1}{H_\alpha^k} \\ 0 & 0 & \frac{1}{H_\beta^k} \\ 0 & 0 & 0 \end{bmatrix} . \quad (42)
$$

After the integration by parts, the governing equations have the following form:

$$
\delta \boldsymbol{u}_\tau^k : \qquad \boldsymbol{K}_{uu}^{k\tau s} \boldsymbol{u}_s^k = \boldsymbol{p}_{u\tau}^k - \boldsymbol{K}_{u\theta}^{k\tau s} \theta_s^k - \boldsymbol{K}_{u\mathcal{M}}^{k\tau s} \mathcal{M}_s^k , \quad (43)
$$

with related boundary conditions on edge Γ_k:

$$
\boldsymbol{\Pi}_{uu}^{k\tau s} \boldsymbol{u}_s^k - \boldsymbol{\Pi}_{\theta\theta}^{k\tau s} \theta_s^k - \boldsymbol{\Pi}_{\mathcal{MM}}^{k\tau s} \mathcal{M}_s^k = \boldsymbol{\Pi}_{uu}^{k\tau s} \bar{\boldsymbol{u}}_s^k - \boldsymbol{\Pi}_{\theta\theta}^{k\tau s} \bar{\theta}_s^k - \boldsymbol{\Pi}_{\mathcal{MM}}^{k\tau s} \bar{\mathcal{M}}_s^k , \quad (44)
$$

where $\boldsymbol{p}_{u\tau}^k$ is the mechanical load, $\boldsymbol{u}_s^k$ is the vector of the degrees of freedom for the displacements, θ_s^k is the vector for the over-temperature approximation, $\mathcal{M}_s^k$ is the vector for the moisture content approximation, $\boldsymbol{K}_{uu}^{k\tau s}$ is the fundamental nucleus for the stiffness matrix, $\boldsymbol{K}_{u\theta}^{k\tau s}$ is the fundamental nucleus for the definition of the thermal load $\boldsymbol{p}_{\theta\tau}^k = -\boldsymbol{K}_{u\theta}^{k\tau s} \theta_s^k$, $\boldsymbol{K}_{u\mathcal{M}}^{k\tau s}$ is the fundamental nucleus for the definition of the hygroscopical load $\boldsymbol{p}_{\mathcal{M}\tau}^k = -\boldsymbol{K}_{u\mathcal{M}}^{k\tau s} \mathcal{M}_s^k$. $\boldsymbol{\Pi}_{uu}^{k\tau s}$, $\boldsymbol{\Pi}_{u\theta}^{k\tau s}$ and $\boldsymbol{\Pi}_{u\mathcal{M}}^{k\tau s}$ are the fundamental nuclei for the boundary conditions:

$$
\boldsymbol{K}_{uu}^{k\tau s} = \int_{A_k} \left(\left(- \boldsymbol{D}_p^k + \boldsymbol{A}_p^k \right)^T \left(\boldsymbol{Q}_{pp}^k (\boldsymbol{D}_p^k + \boldsymbol{A}_p^k) + \boldsymbol{Q}_{pn}^k (\boldsymbol{D}_{np}^k + \boldsymbol{D}_{nz}^k - \boldsymbol{A}_n^k) \right) + \left(- \boldsymbol{D}_{np}^k + \boldsymbol{D}_{nz}^k - \boldsymbol{A}_n^k \right)^T \right.
$$

$$
\left. \left(\boldsymbol{Q}_{np}^k (\boldsymbol{D}_p^k + \boldsymbol{A}_p^k) + \boldsymbol{Q}_{nn}^k (\boldsymbol{D}_{np}^k + \boldsymbol{D}_{nz}^k - \boldsymbol{A}_n^k) \right) \right) F_s F_\tau H_\alpha^k H_\beta^k dz , \quad (45)
$$

$$\boldsymbol{K}_{u\theta}^{k\tau s} = \int\limits_{A_k} \left(\left(-\boldsymbol{D}_p^k + \boldsymbol{A}_p^k \right)^T \left(-\boldsymbol{\lambda}_p^k \right) + \left(-\boldsymbol{D}_{np}^k + \boldsymbol{D}_{nz}^k - \boldsymbol{A}_n^k \right)^T \left(-\boldsymbol{\lambda}_n^k \right) \right) F_s F_\tau H_\alpha^k H_\beta^k dz \ , \qquad (46)$$

$$\boldsymbol{K}_{u\mathcal{M}}^{k\tau s} = \int\limits_{A_k} \left(\left(-\boldsymbol{D}_p^k + \boldsymbol{A}_p^k \right)^T \left(-\boldsymbol{\mu}_p^k \right) + \left(-\boldsymbol{D}_{np}^k + \boldsymbol{D}_{nz}^k - \boldsymbol{A}_n^k \right)^T \left(-\boldsymbol{\mu}_n^k \right) \right) F_s F_\tau H_\alpha^k H_\beta^k dz \ , \qquad (47)$$

$$\boldsymbol{\Pi}_{uu}^{k\tau s} = \int\limits_{A_k} \left(\left(\boldsymbol{I}_p^k \right)^T \left(\boldsymbol{Q}_{pp}^k (\boldsymbol{D}_p^k + \boldsymbol{A}_p^k) + \boldsymbol{Q}_{pn}^k (\boldsymbol{D}_{np}^k + \boldsymbol{D}_{nz}^k - \boldsymbol{A}_n^k) \right) + \left(\boldsymbol{I}_{np}^k \right)^T \right. \qquad (48)$$

$$\left(\boldsymbol{Q}_{np}^k (\boldsymbol{D}_p^k + \boldsymbol{A}_p^k) + \boldsymbol{Q}_{nn}^k (\boldsymbol{D}_{np}^k + \boldsymbol{D}_{nz}^k - \boldsymbol{A}_n^k) \right) \right) F_s F_\tau H_\alpha^k H_\beta^k dz \ ,$$

$$\boldsymbol{\Pi}_{u\theta}^{k\tau s} = \int\limits_{A_k} \left(\left(\boldsymbol{I}_p^k \right)^T \left(-\boldsymbol{\lambda}_p^k \right) + \left(\boldsymbol{I}_{np}^k \right)^T \left(-\boldsymbol{\lambda}_n^k \right) \right) F_s F_\tau H_\alpha^k H_\beta^k dz \ , \qquad (49)$$

$$\boldsymbol{\Pi}_{u\mathcal{M}}^{k\tau s} = \int\limits_{A_k} \left(\left(\boldsymbol{I}_p^k \right)^T \left(-\boldsymbol{\mu}_p^k \right) + \left(\boldsymbol{I}_{np}^k \right)^T \left(-\boldsymbol{\mu}_n^k \right) \right) F_s F_\tau H_\alpha^k H_\beta^k dz \ . \qquad (50)$$

5.2   Fundamental nuclei

In order to write the explicit form of fundamental nuclei in Eqs.(45)-(47), the following integrals in the z thickness-direction can be defined:

$$(J^{k\tau s}, J_\alpha^{k\tau s}, J_\beta^{k\tau s}, J_{\frac{\alpha}{\beta}}^{k\tau s}, J_{\frac{\beta}{\alpha}}^{k\tau s}, J_{\alpha\beta}^{k\tau s}) = \int\limits_{A_k} F_\tau F_s \left(1, H_\alpha^k, H_\beta^k, \frac{H_\alpha^k}{H_\beta^k}, \frac{H_\beta^k}{H_\alpha^k}, H_\alpha^k H_\beta^k \right) dz \ ,$$

$$(J^{k\tau_z s}, J_\alpha^{k\tau_z s}, J_\beta^{k\tau_z s}, J_{\frac{\alpha}{\beta}}^{k\tau_z s}, J_{\frac{\beta}{\alpha}}^{k\tau_z s}, J_{\alpha\beta}^{k\tau_z s}) = \int\limits_{A_k} \frac{\partial F_\tau}{\partial z} F_s \left(1, H_\alpha^k, H_\beta^k, \frac{H_\alpha^k}{H_\beta^k}, \frac{H_\beta^k}{H_\alpha^k}, H_\alpha^k H_\beta^k \right) dz \ , \qquad (51)$$

$$(J^{k\tau s_z}, J_\alpha^{k\tau s_z}, J_\beta^{k\tau s_z}, J_{\frac{\alpha}{\beta}}^{k\tau s_z}, J_{\frac{\beta}{\alpha}}^{k\tau s_z}, J_{\alpha\beta}^{k\tau s_z}) = \int\limits_{A_k} F_\tau \frac{\partial F_s}{\partial z} \left(1, H_\alpha^k, H_\beta^k, \frac{H_\alpha^k}{H_\beta^k}, \frac{H_\beta^k}{H_\alpha^k}, H_\alpha^k H_\beta^k \right) dz \ ,$$

$$(J^{k\tau_z s_z}, J_\alpha^{k\tau_z s_z}, J_\beta^{k\tau_z s_z}, J_{\frac{\alpha}{\beta}}^{k\tau_z s_z}, J_{\frac{\beta}{\alpha}}^{k\tau_z s_z}, J_{\alpha\beta}^{k\tau_z s_z}) = \int\limits_{A_k} \frac{\partial F_\tau}{\partial z} \frac{\partial F_s}{\partial z} \left(1, H_\alpha^k, H_\beta^k, \frac{H_\alpha^k}{H_\beta^k}, \frac{H_\beta^k}{H_\alpha^k}, H_\alpha^k H_\beta^k \right) dz \ .$$

By using the Eqs.(51), by developing the matrix products in Eqs.(45)-(47) and employing a Navier-type closed form solution [10]-[12], the algebraic explicit form of the nuclei can be obtained.
The nucleus $\boldsymbol{K}_{uu}^{k\tau s}$ has 3×3 dimension:

$$K_{uu_{11}}^{k\tau s} = Q_{55}^k J_{\alpha\beta}^{k\tau_z s_z} + Q_{11}^k J_{\frac{\beta}{\alpha}}^{k\tau s} \bar{\alpha}^2 + Q_{66}^k J_{\frac{\alpha}{\beta}}^{k\tau s} \bar{\beta}^2 + Q_{55}^k J_{\frac{\beta}{\alpha}}^{k\tau s} \frac{1}{R_\alpha^{k^2}} - Q_{55}^k J_\beta^{k\tau_z s} \frac{1}{R_\alpha^k} - Q_{55}^k J_\beta^{k\tau s_z} \frac{1}{R_\beta^k} \ ,$$

$$K_{uu_{12}}^{k\tau s} = J^{k\tau s} \bar{\alpha}\bar{\beta} (Q_{12}^k + Q_{66}^k) \ ,$$

$$K_{uu_{13}}^{k\tau s} = -Q_{13}^k J_\beta^{k\tau s_z} \bar{\alpha} + Q_{55}^k J_\beta^{k\tau_z s} \bar{\alpha} - Q_{11}^k J_{\frac{\beta}{\alpha}}^{k\tau s} \frac{1}{R_\alpha^k} \bar{\alpha} - Q_{12}^k J^{k\tau s} \frac{1}{R_\beta^k} \bar{\alpha} - Q_{55}^k J_{\frac{\beta}{\alpha}}^{k\tau s} \frac{1}{R_\alpha^k} \bar{\alpha} \ ,$$

$$K_{uu_{21}}^{k\tau s} = J^{k\tau s} \bar{\alpha}\bar{\beta} (Q_{12}^k + Q_{66}^k)$$

$$K_{uu_{22}}^{k\tau s} = Q_{44}^k J_{\alpha\beta}^{k\tau_z s_z} + Q_{22}^k J_{\frac{\alpha}{\beta}}^{k\tau s} \bar{\beta}^2 + Q_{66}^k J_{\frac{\beta}{\alpha}}^{k\tau s} \bar{\alpha}^2 + Q_{44}^k J_{\frac{\alpha}{\beta}}^{k\tau s} \frac{1}{R_\beta^{k^2}} - Q_{44}^k J_\alpha^{k\tau_z s} \frac{1}{R_\beta^k} - Q_{44}^k J_\alpha^{k\tau s_z} \frac{1}{R_\beta^k} \ , \qquad (52)$$

$$K_{uu_{23}}^{k\tau s} = Q_{44}^k J_\alpha^{k\tau_z s} \bar{\beta} - Q_{23}^k J_\alpha^{k\tau s_z} \bar{\beta} - Q_{12}^k J^{k\tau s} \bar{\beta} \frac{1}{R_\alpha^k} - Q_{22}^k J_{\frac{\alpha}{\beta}}^{k\tau s} \bar{\beta} \frac{1}{R_\beta^k} - Q_{44}^k J_{\frac{\alpha}{\beta}}^{k\tau s} \bar{\beta} \frac{1}{R_\beta^k} \ ,$$

$$K_{uu31}^{k\tau s} = Q_{55}^k J_\beta^{k\tau s_z} \bar{\alpha} - Q_{13}^k J_\beta^{k\tau_z s} \bar{\alpha} - Q_{11}^k J_{\frac{\beta}{\alpha}}^{k\tau s} \bar{\alpha} \frac{1}{R_\alpha^k} - Q_{12}^k J^{k\tau s} \bar{\alpha} \frac{1}{R_\beta^k} - Q_{55}^k J_{\frac{\beta}{\alpha}}^{k\tau s} \bar{\alpha} \frac{1}{R_\alpha^k} ,$$

$$K_{uu32}^{k\tau s} = Q_{44}^k J_\alpha^{k\tau s_z} \bar{\beta} - Q_{23}^k J_\alpha^{k\tau_z s} \bar{\beta} - Q_{12}^k J^{k\tau s} \bar{\beta} \frac{1}{R_\alpha^k} - Q_{22}^k J_{\frac{\alpha}{\beta}}^{k\tau s} \bar{\beta} \frac{1}{R_\beta^k} - Q_{44}^k J_{\frac{\alpha}{\beta}}^{k\tau s} \bar{\beta} \frac{1}{R_\beta^k} ,$$

$$K_{uu33}^{k\tau s} = Q_{55}^k J_{\frac{\beta}{\alpha}}^{k\tau s} \bar{\alpha}^2 + Q_{44}^k J_{\frac{\alpha}{\beta}}^{k\tau s} \bar{\beta}^2 + Q_{33}^k J_{\alpha\beta}^{k\tau_z s_z} + Q_{11}^k J_{\frac{\beta}{\alpha}}^{k\tau s} \frac{1}{R_\alpha^{k\,2}} + 2Q_{12}^k J^{k\tau s} \frac{1}{R_\alpha^k R_\beta^k} + Q_{22}^k J_{\frac{\alpha}{\beta}}^{k\tau s} \frac{1}{R_\beta^{k\,2}}$$
$$+ Q_{13}^k J_\beta^{k\tau_z s} \frac{1}{R_\alpha^k} + Q_{23}^k J_\alpha^{k\tau_z s} \frac{1}{R_\beta^k} + Q_{13}^k J_\beta^{k\tau s_z} \frac{1}{R_\alpha^k} + Q_{23}^k J_\alpha^{k\tau s_z} \frac{1}{R_\beta^k}$$

The nucleus $\boldsymbol{K}_{u\theta}^{k\tau s}$ has 3×1 dimension:

$$K_{u\theta 11}^{k\tau s} = \bar{\alpha} J_\beta^{k\tau s} \lambda_{11}^k , \qquad K_{u\theta 21}^{k\tau s} = \bar{\beta} J_\alpha^{k\tau s} \lambda_{22}^k , \qquad K_{u\theta 31}^{k\tau s} = -J_\beta^{k\tau s} \lambda_{11}^k \frac{1}{R_\alpha^k} - J_\alpha^{k\tau s} \lambda_{22}^k \frac{1}{R_\beta^k} - J_{\alpha\beta}^{k\tau_z s} \lambda_{33}^k . \quad (53)$$

The nucleus $\boldsymbol{K}_{u\mathcal{M}}^{k\tau s}$ has 3×1 dimension:

$$K_{u\mathcal{M} 11}^{k\tau s} = \bar{\alpha} J_\beta^{k\tau s} \mu_{11}^k , \quad K_{u\mathcal{M} 21}^{k\tau s} = \bar{\beta} J_\alpha^{k\tau s} \mu_{22}^k , \quad K_{u\mathcal{M} 31}^{k\tau s} = -J_\beta^{k\tau s} \mu_{11}^k \frac{1}{R_\alpha^k} - J_\alpha^{k\tau s} \mu_{22}^k \frac{1}{R_\beta^k} - J_{\alpha\beta}^{k\tau_z s} \mu_{33}^k . \quad (54)$$

$\bar{\alpha} = m\pi/a$ and $\bar{\beta} = n\pi/b$, with m and n as the wave numbers in in-plane directions, and a and b as the shell dimensions in α and β directions, respectively.

Navier-type closed form solution is obtained via substitution of harmonic expressions for the displacements, over-temperature and moisture content as well as considering the following material coefficients equal to zero: $Q_{16}^k = Q_{26}^k = Q_{36}^k = Q_{45}^k = 0$, and $\alpha_{12}^k = \beta_{12}^k = 0$ which also means $\lambda_{12}^k = \mu_{12}^k = 0$. The following harmonic assumptions are made for the variables, they correspond to simply supported boundary conditions:

$$u_s^k = \sum_{m,n} (\hat{u}_s^k) \cos\left(\frac{m\pi\alpha}{a}\right) \sin\left(\frac{n\pi\beta}{b}\right) , \qquad k = 1, \ldots, N_l ,$$

$$v_s^k = \sum_{m,n} (\hat{v}_s^k) \sin\left(\frac{m\pi\alpha}{a}\right) \cos\left(\frac{n\pi\beta}{b}\right) , \qquad s = t, b, r , \qquad (55)$$

$$(w_s^k, \theta_s^k, \mathcal{M}_s^k) = \sum_{m,n} (\hat{w}_s^k, \hat{\theta}_s^k, \hat{\mathcal{M}}_s^k) \sin\left(\frac{m\pi\alpha}{a}\right) \sin\left(\frac{n\pi\beta}{b}\right) , \qquad r = 2, \ldots, N ,$$

where $\hat{u}_s^k$, $\hat{v}_s^k$, $\hat{w}_s^k$, $\hat{\theta}_s^k$ and $\hat{\mathcal{M}}_s^k$ are the amplitudes, k indicates the layer, s is the order of expansion which considers top (t), bottom (b) and higher order of expansion from $N = 2$ to $N = 4$. $s = 0, \ldots, 4$ in the case of ESL approach for displacement components.

By starting from the 3×3 fundamental nucleus in Eq.(52), the stiffness matrix of the considered multilayered shell is obtained by expanding via the indexes τ and s for the order of expansion in the thickness direction and via the index k for the multilayer assembling procedure (Equivalent Single Layer (ESL) or Layer Wise (LW)). The procedure is the same for the fundamental nuclei in Eqs.(53) and (54) where θ_s^k and $\mathcal{M}_s^k$ are always given in LW form. Further details about the assembling procedure can be found in [38].

5.3 Mechanical, thermal and hygroscopic loads

In the governing relations proposed in Eq.(43), the mechanical load is applied as a pressure in the transverse direction at the top or at the bottom of the multilayered shell in harmonic form:

$$p_z(\alpha, \beta, z) = \hat{p}_z(z) \sin(\frac{m\pi}{a}\alpha) \sin(\frac{n\pi}{b}\beta) , \qquad (56)$$

where the amplitudes can be $\hat{p}_z(+h/2) = \hat{p}_{ztop}$ or $\hat{p}_z(-h/2) = \hat{p}_{zbot}$. When the multilayered shell is in a thermo-hygroscopic environment, a temperature profile and a moisture content profile are generated through the thickness, their form in the plane directions are:

$$\theta(\alpha, \beta, z) = \hat{\theta}(z) \sin(\frac{m\pi}{a}\alpha) \sin(\frac{n\pi}{b}\beta) \,, \tag{57}$$

$$\mathcal{M}(\alpha, \beta, z) = \hat{\mathcal{M}}(z) \sin(\frac{m\pi}{a}\alpha) \sin(\frac{n\pi}{b}\beta) \,. \tag{58}$$

These profiles give a thermal load $\boldsymbol{p}_{\theta\tau}^k = -\boldsymbol{K}_{u\theta}^{k\tau s}\theta_s^k$ and an hygroscopic load $\boldsymbol{p}_{\mathcal{M}\tau}^k = -\boldsymbol{K}_{u\mathcal{M}}^{k\tau s}\mathcal{M}_s^k$. Such loads are defined when the two profiles are known through the z thickness direction and then they are approximated via the Carrera's Unified Formulation (CUF). Three different cases are possible: the first case considers a constant temperature and/or moisture content profile through the thickness direction from the top to the bottom of the shell, in this case the profiles are a priori known and it is easy to introduce them in the CUF; the second case considers a gradient for the temperature and/or the moisture content, their values are known at the top and bottom of the shell and linear profiles are "a priori" assumed and introduced in the CUF; the third case has the same gradient for the temperature and/or the moisture content of the case two, but now the profiles are calculated by means of the Fourier heat conduction equation (over-temperature) and the Fick moisture diffusion law (moisture content). These calculated profiles could be different from the assumed linear ones for thick and/or multilayered anisotropic shells.

The Fourier heat conduction equation for curvilinear coordinates is:

$$\left(\frac{\kappa_{11}^k}{H_\alpha^{k2}}\right) \frac{\partial^2\theta}{\partial\alpha^2} + \left(\frac{\kappa_{22}^k}{H_\beta^{k2}}\right) \frac{\partial^2\theta}{\partial\beta^2} + \kappa_{33}^k \frac{\partial^2\theta}{\partial z^2} = 0 \,, \tag{59}$$

at steady-state conditions the term $\frac{\partial\theta}{\partial t}$ is zero. θ is the over-temperature of T_1 referred to the external room reference temperature T_0. κ_{11}^k, κ_{22}^k and κ_{33}^k are the thermal conductivity coefficients for each kth layer. H_α^k and H_β^k are the metric coefficients depending on the thickness coordinate and on the radii of curvature, for such a reason the Eq.(59) has not constant coefficients and it is solved by means of mathematical layers as suggested in [10], [11] and [12] (see these papers for further details about the solution procedure). We compute the over-temperature amplitude at different values z_N of the thickness coordinate, the N values of θ_s^k for the CUF in Eq.(35) are obtained by solving the system in Eq.(60):

$$\begin{bmatrix} \hat{\theta}_c(z_1) \\ \hat{\theta}_c(z_2) \\ \vdots \\ \hat{\theta}_c(z_N) \end{bmatrix} = \begin{bmatrix} F_0(z_1) & F_1(z_1) & \cdots & F_N(z_1) \\ F_0(z_2) & F_1(z_2) & \cdots & F_N(z_2) \\ \vdots & \vdots & \vdots & \vdots \\ F_0(z_N) & F_1(z_N) & \cdots & F_N(z_N) \end{bmatrix} \begin{bmatrix} \theta_0^k \\ \theta_1^k \\ \vdots \\ \vdots \\ \theta_N^k \end{bmatrix} \,. \tag{60}$$

Therefore, the over-temperature profile in a generic multilayered shell is approximated by Eq.(35) and the N values of θ_s^k are given by the solution of the system in Eq.(60).

The Fick diffusion law is solved in analogy with the Fourier heat conduction equation and for curvilinear coordinates it reads as (see the plate case in [2]):

$$\left(\frac{\mathcal{D}_{11}^k}{H_\alpha^{k2}}\right) \frac{\partial^2\mathcal{M}}{\partial\alpha^2} + \left(\frac{\mathcal{D}_{22}^k}{H_\beta^{k2}}\right) \frac{\partial^2\mathcal{M}}{\partial\beta^2} + \mathcal{D}_{33}^k \frac{\partial^2\mathcal{M}}{\partial z^2} = 0 \,, \tag{61}$$

at steady-state conditions the term $\frac{\partial\mathcal{M}}{\partial t}$ is zero. $\mathcal{M}$ is the the moisture content. $\mathcal{D}_{11}^k$, $\mathcal{D}_{22}^k$ and $\mathcal{D}_{33}^k$ are the diffusion coefficients for each kth layer. The Eq.(61) has not constant coefficients and it is solved

by means of mathematical layers as suggested in [10], [11] and [12] (see these papers for further details about the solution procedure). We compute the moisture content amplitude at different values z_N of the thickness coordinate, and the N values of $\mathcal{M}_s^k$ for the CUF in Eq.(36) are obtained from the solution of the system in Eq.(62):

$$
\begin{bmatrix}
\hat{\mathcal{M}}_c(z_1) \\
\hat{\mathcal{M}}_c(z_2) \\
\vdots \\
\hat{\mathcal{M}}_c(z_N)
\end{bmatrix}
=
\begin{bmatrix}
F_0(z_1) & F_1(z_1) & \cdots & F_N(z_1) \\
F_0(z_2) & F_1(z_2) & \cdots & F_N(z_2) \\
\vdots & \vdots & \vdots & \vdots \\
F_0(z_N) & F_1(z_N) & \cdots & F_N(z_N)
\end{bmatrix}
\begin{bmatrix}
\mathcal{M}_0^k \\
\mathcal{M}_1^k \\
\vdots \\
\vdots \\
\mathcal{M}_N^k
\end{bmatrix} .
\tag{62}
$$

Therefore, the moisture content profile in a generic multilayered shell is approximated by Eq.(36) and the N values of $\mathcal{M}_s^k$ are given by the solution of the system in Eq.(62).

6 Results

The effects of temperature and moisture content are investigated in simply supported multilayered composite and sandwich shells when they are subjected to an harmonic transverse pressure applied at the top. The static response in terms of displacements and stresses changes because such fields generate equivalent loads. The benchmarks proposed consider the bending problem of a two-layered composite cylindrical shell panel and a sandwich shell panel (bi-sinusoidal transverse pressure applied at the top) in thermo-hygroscopic environment. Such a condition can be represented by a constant through-the-thickness over-temperature or moisture content profile, or by a through-the-thickness gradient for the over-temperature or moisture content (in this second case the profiles can linearly be assumed or they can be calculated by solving the Eqs. (59) and (61), respectively). These benchmarks are analyzed after some preliminary assessments which confirm the validity of the refined CUF shell models when the multilayered structures are subjected to a mechanical load, to an imposed over-temperature and to an imposed moisture content, separately. The refined LW models give a satisfactory and quasi-3D analysis for each considered load, thickness ratio and lamination sequence, and they can be used as reference solutions in the benchmark proposed.

6.1 Assessments

The first assessment considers a simply supported two-layered curved panel, in cylindrical bending, with a mechanical load applied at its top surface:

$$
p_{ztop}(\alpha, \beta) = \hat{p}_z \sin \frac{m\pi\alpha}{a} \ ,
\tag{63}
$$

with the amplitude $\hat{p}_z = 1 \ psi$ and waves number in α-direction $m = 1$. It is made of two layers of equal thickness $h_1 = h_2 = 0.5h$, material properties are Young modulii $E_1 = 25 \times 10^6 psi$ and $E_2 = E_3 = 1 \times 10^6 psi$, shear modulii $G_{12} = G_{13} = 0.5 \times 10^6 psi$ and $G_{23} = 0.2 \times 10^6 psi$, Poisson ratio $\nu_{12} = \nu_{13} = \nu_{23} = 0.25$. The lamination sequence is $90°/0°$, the geometry is that indicated in Figure 2 with radius of curvature in β direction $R_\beta = \infty$, the radius of curvature in α direction is $R_\alpha = 10$ with angle Φ equals $\frac{\pi}{3}$, the two dimensions of the panel are $a = \frac{\pi}{3}R_\alpha$ and $b = 1$. The maximum stresses and deflections are given in Table 1 in non-dimensional form:

$$
(\bar{\sigma}_{\alpha\alpha}, \bar{\sigma}_{\beta\beta}) = \frac{(\sigma_{\alpha\alpha}, \sigma_{\beta\beta})}{\hat{p}_z(\frac{R_\alpha}{h})^2} \ , \quad (\bar{\sigma}_{\alpha z}) = \frac{(\sigma_{\alpha z})}{\hat{p}_z(\frac{R_\alpha}{h})} \ , \quad \bar{w} = \frac{10 E_1 w}{\hat{p}_z h(\frac{R_\alpha}{h})^4} \ ,
\tag{64}
$$

13

the exact 3D solution has been proposed by Ren [39] and it is compared with some classical and refined two-dimensional models based on CUF for thickness ratios R_α/h equals 10 (thick shell) and 500 (thin shell). It is clear how the refined LW CUF model (LD4 in this example) always gives the 3D evaluation in terms of displacements and stresses for each thickness ratio. LD4 model can be considered as a quasi-3D solution in the case of static investigation of multilayered shells subjected to mechanical loads. Refined ESL models give some problems for the stress evaluation (in particular for thick shells), classical models (CLT and FSDT) are often inadequate.

The second assessment considers a simply supported cylindrical shell panel with ten carbon fiber reinforced layers with lamination sequence $(0°/90°)_k$. The proposed shell has dimensions $a = b = 1$. The radii of curvature in the α and β directions are $\frac{1}{R_\alpha} = 0$ and $\frac{1}{R_\beta} = 0.2, 0.1, 0.02$, the total thicknesses is $h = 0.1$. The ratio between Young modulus in the longitudinal and transverse directions is $E_L/E_T = 25.0$. The shear modulus ratio is $G_{LT}/G_{TT} = 2.5$, Poisson ratio is $\nu_{LT} = \nu_{TT} = 0.25$. The ratio between the thermal expansion coefficient in the transverse and longitudinal directions is $\alpha_T/\alpha_L = 3.0$. The conductivity coefficients are $\kappa_L = 36.42 W/mK$ in the longitudinal direction and $\kappa_T = 0.96 W/mK$ in the transverse direction. Each layer has thickness equals $h/10$. The results for the non-dimensional transverse displacement $\bar{w} = \frac{w}{b^2 \alpha_L \Delta\theta}$ in $z = 0$ are given in Table 2. The shell has an imposed over-temperature at the top $\theta_{top} = +0.5K$ and an imposed over-temperature at the bottom $\theta_{bot} = -0.5K$, this means a temperature gradient $\Delta\theta = 1K$. Khare et alii [40] have proposed an higher shear deformation theory called HOST12 where the temperature is linearly assumed through the thickness from the $+0.5K$ top value to the $-0.5K$ bottom value. The CUF models proposed can use both assumed θ_a and calculated θ_c temperature profiles, the refined models with assumed temperature profile gives results which are very close to the HOST12 model [40]. However the shell is multilayered and the use of a calculated temperature profile is suitable. FSDT and CLT classical models give results which are not close to the quasi-3D evaluation. The 10 layers are made of the same material and only the fibre orientation changes, this means that refined models must be used but the use of LW approaches is not mandatory as in the sandwich case.

The third assessment considers a simply supported square plate with thickness ratio $a/h = 5$. The multilayered plate is in fibre reinforced composite material with lamination sequence $0°/90°/0°/90°$, each layer thickness is $h_1 = h_2 = h_3 = h_4 = h/4$ with total thickness $h = 1$. The moisture content is applied as harmonic in in-plane directions with wave numbers $m = n = 1$, and it is constant through the thickness direction. Displacement and stress amplitudes are given as $(\sigma_{xx}^*, \sigma_{yy}^*, \sigma_{xy}^*, \sigma_{xz}^*, \sigma_{yz}^*) = \frac{(\sigma_{xx}, \sigma_{yy}, \sigma_{xy}, \sigma_{xz}, \sigma_{yz})}{\mathcal{M}_0 E_0}$ and $(u^*, v^*, w^*) = \frac{(u,v,w)}{\mathcal{M}_0}$ with $E_0 = 1GPa$ and $\mathcal{M}_0 = 0.0025$. Material properties for moisture content $\mathcal{M} = 0.0$ are Young modulii $E_1 = 130GPa$ and $E_2 = E_3 = 9.5GPa$, shear modulii $G_{12} = G_{13} = 6GPa$ and $G_{23} = 3GPa$, Poisson ratios $\nu_{12} = \nu_{13} = \nu_{23} = 0.3$ and moisture expansion coefficients $\beta_{11} = 0.0$ and $\beta_{22} = \beta_{33} = 0.44$. When the moisture content increases, the transverse Young modulus decreases (the other properties do not change), therefore $E_2 = E_3 = 9.25GPa$ for $\mathcal{M} = 0.0025$, $E_2 = E_3 = 9.0GPa$ for $\mathcal{M} = 0.005$, $E_2 = E_3 = 8.75GPa$ for $\mathcal{M} = 0.0075$, $E_2 = E_3 = 8.5GPa$ for $\mathcal{M} = 0.01$, $\mathcal{M} = 0.0125$ and $\mathcal{M} = 0.0150$. Figure 3 proposes displacements and stresses evaluation through the thickness of the multialyered plate when the constant moisture content increases (the material properties also change), the LD4 model gives a satisfactory analysis and it is in accordance with the higher order theory proposed by Lo et alii [13] which gives the same through-the-thickness evaluation of these variables.

The three assessments proposed in this section have demonstrated how refined CUF models give a correct evaluation of multilayered plate and shell structures when they are subjected to mechanical pressure, imposed over-temperature at the external surfaces and imposed moisture content. In particular, the LD4 model gives a quasi-3D evaluation in terms of displacements and stresses for each geometry, thickness ratio, lamination sequence and load conditions, and it can be used as a reference solution in the new benchmarks proposed.

6.2 Benchmarks

The new benchmarks consider a simply supported cylindrical shell panel (see Figure 2) where a transverse mechanical pressure is applied at its top surface in harmonic form $p_z(\alpha, \beta, z) = \hat{p}_z(z)sin(\frac{m\pi\alpha}{a})sin(\frac{n\pi\beta}{b})$. The amplitude value is $\hat{p}_z = 10000Pa$ with wave numbers $m = n = 1$ in both α and β directions. The shell has radii of curvature $R_\alpha = 10$ in α direction and $R_\beta = \infty$ in β direction, and dimensions $a = \frac{\pi}{3}R_\alpha = 10.47197551$ and $b = 1$. The thickness ratios investigated are $R_\alpha/h = 10$ that means total thickness $h = 1$ and $R_\alpha/h = 500$ that means total thickness $h = 0.02$. The hygrothermal environmental conditions could be given as through-the-thickness temperature or moisture content profiles which are bi-sinusoidal in the $\alpha\beta$-plane (wave numbers $m = n = 1$).

The first benchmark configuration is a two-layered composite shell with fiber orientation $0°/90°$ and layer thickness $h_1 = h_2 = 0.5h$ (from the bottom to the top). The fibre reinforced composite material has Young modulii $E_1 = 138GPa$ and $E_2 = E_3 = 8.5GPa$, shear modulii $G_{12} = G_{13} = 4.5GPa$ and $G_{23} = 3.2GPa$, Poisson ratios $\nu_{12} = \nu_{13} = 0.29$ and $\nu_{23} = 0.36$, thermal expansion coefficients $\alpha_{11} = -0.5 \times 10^{-6}K^{-1}$ and $\alpha_{22} = \alpha_{33} = 43 \times 10^{-6}K^{-1}$, conductivity coefficients $\kappa_{11} = 4.2W/mK$ and $\kappa_{22} = \kappa_{33} = 0.7W/mK$, moisture expansion coefficients $\beta_{11} = 0$ and $\beta_{22} = \beta_{33} = 0.4 \times 10^{-2}$ (in this form when the moisture content is given in percentage), moisture diffusion coefficients $\mathcal{D}_{11} = 4.4 \times 10^{-3}m^2/s$ and $\mathcal{D}_{22} = \mathcal{D}_{33} = 3.1 \times 10^{-3}m^2/s$ (when in the Fick law we use the moisture concentration c in $[kg/m^3]$) or moisture diffusion coefficients $\mathcal{D}_{11} = 7.04kg/ms$ and $\mathcal{D}_{22} = \mathcal{D}_{33} = 4.96kg/ms$ (when in the Fick law we use the moisture content $\mathcal{M}$, we have multiplied by the mass density $\rho = 1600kg/m^3$).

The second benchmark configuration is a five-layered sandwich shell with lamination sequence (from the bottom to the top) $0°/90°/core/90°/0°$ and layer thickness $h_1 = h_2 = h_4 = h_5 = 0.1h$ and $h_3 = 0.6h$. The four external composite layers have the same hygrothermoelastic properties already given in the first benchmark, the central soft core has Young modulus $E = 3GPa$, Poisson ratio $\nu = 0.4$, thermal expansion coefficient $\alpha = 50 \times 10^{-6}K^{-1}$, conductivity coefficient $\kappa = 0.18W/mK$, moisture expansion coefficient $\beta = 0.28 \times 10^{-2}$ (in this form when the moisture content is given in percentage), moisture diffusion coefficient $\mathcal{D} = 6.66 \times 10^{-11}m^2/s$ (when in the Fick law we use the moisture concentration c in $[kg/m^3]$) or moisture diffusion coefficient $\mathcal{D} = 9.324 \times 10^{-8}kg/ms$ (when in the Fick law we use the moisture content $\mathcal{M}$, we have multiplied by the mass density $\rho = 1400kg/m^3$).

In both benchmarks the hygothermal environmental conditions can be given as constant through-the-thickness temperature profile (an over-temperature with respect to the reference temperature equals $(\theta_a = 50K)$), linear through-the-thickness temperature profile (from $50K$ at the top to $0K$ at the bottom, $(\theta_a = 50K, 0K)$), calculated through-the-thickness temperature profile (from $50K$ at the top to $0K$ at the bottom, $(\theta_c = 50K, 0K)$, by solving the Fourier heat conduction equation), constant through-the-thickness moisture content profile $(\mathcal{M}_a = 0.5\%)$, linear through-the-thickness moisture content profile (from 0.5% at the top to 0.1% at the bottom, $(\mathcal{M}_a = 0.5\%, 0.1\%)$), calculated through-the-thickness moisture content profile (from 0.5% at the top to 0.1% at the bottom, $(\mathcal{M}_c = 0.5\%, 0.1\%)$, by solving the Fick diffusion law).

The results for the two-layered composite shell are given in Tables 3 and 4 in terms of transverse displacement, in-plane normal stress, in-plane shear stress and transverse shear stress. The refined LW model LD4 gives a quasi-3D description in the case of mechanical pressure, the refined ESL model ED4 has some difficulties for the thick case ($R_\alpha/h = 10$ in Tables 3, in particular for the stress evaluation) even if it is very close to LD4 model for the thin configuration in Table 4 ($R_\alpha/h = 500$) for both displacement and stress evaluations. Classical models, such as FSDT and CLT, are inadequate for the thick shell while they appears quite good for the thin configuration even if some problems are shown for the stress evaluation (for example the CLT model does not give any information about the transverse shear stress). This preliminary analysis about the pure mechanical case suggests only the use of ED4 and LD4 models for the evaluation of the hygroscopic effects in such structures. When a constant through-the-thickness temperature profile is added to the mechanical load, a bigger transverse displacement and bigger stresses are obtained; such increments are smaller when the temperature

has a gradient from $50K$ at the top to $0K$ at the bottom, in the case of thick shell (Table 3) the assumption of a linear temperature profile is wrong and such a profile must be calculated by solving the Fourier heat conduction equation. When the shell is thin (Table 4) the temperature profile is linear through the thickness even if the two layers have different fibre orientation which only affects the in-plane conductivity coefficients (see comparison between $LD4(\theta_a = 50K, 0K)$ and $LD4(\theta_c = 50K, 0K)$ models). A constant through-the-thickness moisture content profile $\mathcal{M}_a = 0.5\%$ has similar effects to those obtained with the constant temperature profile, in this case a comparison between LD4 and ED4 models has been added, the ED4 model works quite well for thin shell (Table 4) but it has some difficulties for the thick case (Table 3) for both displacement and stress evaluation. When a moisture content gradient is imposed on the surfaces of the shells, the ESL and LW models can use an assumed linear profile or they can calculate it by solving the diffusion Fick law. When the shell is thin ($R_\alpha/h = 500$ in Tables 4) the ED4 and LD4 model are quite similar for both displacement and stress evaluation and the moisture content profile can be considered as linear through the thickness, but in the case of thick shell ($R_\alpha/h = 10$ in Tables 3) the use of LD4 model is mandatory for a quasi-3D description in terms of stress and displacement and the moisture content profile must be calculated because it is not linear through the thickness. By considering the $LD4(\mathcal{M}_c = 0.5\%, 0.1\%)$ model, it is clear how the presence of an hygroscopic environment allows bigger displacements to be obtained and the relative stresses also change.

The results for the five-layered sandwich shell are given in Tables 5 and 6 in terms of transverse displacement, in-plane normal stress, in-plane shear stress and transverse shear stress. The refined LW model LD4 gives a quasi-3D description in the case of mechanical pressure, the refined ESL model ED4 has some difficulties for both thick and thin cases ($R_\alpha/h = 10$ in Table 5 and $R_\alpha/h = 500$ in Table 6) because of the high transverse anisotropy of this configuration (zigzag effect for displacements due to the presence of the central soft core). For the same reason, the use of classical models, such as FSDT and CLT, are inadequate for each thickness ratio and variable analyzed. This preliminary analysis confirms that a quasi-3D description of the mechanical bending of sandwich shells, in terms of displacements and stresses, is only possible via the LD4 model. When a constant through-the-thickness temperature profile is added to the mechanical load, a bigger transverse displacement and bigger stresses are obtained; such increments are smaller when the temperature has a gradient from $50K$ at the top to $0K$ at the bottom, the assumption of linear temperature profile is always wrong for both thick and thin shells because in the sandwich configuration the layers have different conductivity coefficients and the slope of the profile changes in each layer, for this reason the temperature profile must be always calculated by solving the Fourier heat conduction equation (see comparison between $LD4(\theta_a = 50K, 0K)$ and $LD4(\theta_c = 50K, 0K)$ models in Tables 5 and 6 for both thick and thin structures). A constant through-the-thickness moisture content profile $\mathcal{M}_a = 0.5\%$ has similar effects to those obtained with the constant temperature profile, the LD4 model works better than the ED4 one because it captures the zigzag effects typical of sandwich structures. When a moisture content gradient is imposed on the surfaces of the shells, the ESL and LW models can use an assumed linear profile or they can calculate it by solving the diffusion Fick law. In the case of sandwich shells the use of a calculated moisture content profile is always mandatory for both thick and thin shells because such a profile is never linear due to the different diffusivity coefficients of core and skin layers. The quasi-3D hygrothermoleastic analysis of sandwich shells is only possible if an LD4 model is employed and an actual moisture content profile is calculated. It is clear how the presence of an hygroscopic environment allows bigger displacements to be obtained and the relative stresses also change (see the results obtained by means of the $LD4(\mathcal{M}_c = 0.5\%, 0.1\%)$ model).

Figure 4 gives the comparison between the constant through-the-thickness temperature profile, the assumed linear one and the calculated temperature profile for thin shells (two-layered composite structure on the left and five-layered sandwich structure on the right), for sandwich structures the temperature profile is never linear because in the solution of the Fourier heat conduction equation the core has

16

a conductivity coefficient completely different from those of the skins. The same considerations can be made for the comparison between constant through-the-thickness moisture content profile, the assumed linear profile and the calculated moisture content profile for thin shells in Figure 5 (two-layered composite structure on the left and five-layered sandwich structure on the right), for sandwich structures the conclusions are the same already seen for the temperature (use of the analogy between the Fourier heat conduction equation and the Fick diffusion law, and between the conductivity coefficients and the diffusion ones). Figure 6 considers thick composite and sandwich shells, the transverse displacement obtained in the case of pure mechanical load is compared with the cases when a constant through-the-thickness, assumed linear and calculated moisture content profiles are added; it is clear how the LD4 model gives a quasi-3D description in terms of displacements. Such a quasi-3D description is also given for the transverse shear stress evaluation made in Figure 7 for both thin composite and sandwich shells. The use of LW models is mandatory and the moisture content profile gives big changes in the stress evaluation.

7   Conclusions

Multilayered composite and sandwich shells have been analyzed in the case of bending problem in hygrothermal environment. The thermal and hygroscopic effects have been introduced by means of the imposition of over-temperature and moisture content at the external surfaces of the shell, their profiles trough the thickness of the shell can "a priori" be assumed or they can be calculated by solving the Fourier heat conduction equation (for the temperature profile) and the Fick diffusion law (for the moisture content profile). Such equations have been written in curvilinear coordinates for shells, they have been solved by means of mathematical layers and by using the analogy between the Fick law and the Fourier heat conduction equation. Such profiles give equivalent thermal and hygroscopic loads which make worse the bending response of the shells in terms of displacements and stresses. Refined two-dimensional models have been developed for the shell geometry by means of the Carrera's Unified Formulation (both ESL and LW multilayer approaches) and these models are mandatory with respect to classical ones (FSDT and CLT) in order to evaluate hygrothermal effects. In conclusion, the use of refined layer-wise models combined with calculated temperature and moisture content profiles is mandatory for thick and/or sandwich shells with transverse anisotropy.

References

[1] H. Bouadi, *Hygrothermal Effects on Complex Moduli of Composite Laminates*, Ph.D. Dissertation, University of Florida, 1988.

[2] S. Brischetto and E. Carrera, Hygrothermal loading effects in bending analysis of multilayered composite plates, *Journal of Composite Materials*, submitted, 2012.

[3] S.W. Tsai, *Composites Design*, Think Composites, Dayton, OH, 1986.

[4] J.N. Reddy, *Mechanics of Laminated Composite Plates and Shells. Theory and Analysis*, Second Edition, CRC Press, Boca Raton (Florida) 2004.

[5] A. Szekeres, Analogy between heat and moisture thermo-hygro-mechanical tailoring of composites by taking into account the second sound phenomenon, *Computers and Structures*, 76, 145-152, 2000.

[6] A.A.O. Tay and K.Y. Goh, A Study of delamination growth in the die-attach layer of plastic IC packages under hygrothermal loading during solder reflow, *IEEE Transactions on Device and Materials Reliability*, 3, 144-151, 2003.

[7] A.A.O. Tay and K.Y. Goh, A study of delamination growth in the die-attach layer of plastic IC packages under hygrothermal loading during solder reflow, *Electronic Components and Technology Conference, 1999. 1999 Proceedings. 49th*, 694-701, 1999.

[8] R. Di Domizio, A. Lupulescu and M.E. Glicksman, Simulation of Fick's Verification of the 2nd Law, *Journal for the Basic Principles of Diffusion Theory, Experiment and Application*, 4, 1-14, 2006.

[9] V. Tungikar and B.K.M. Rao, Three dimensional exact solution of thermal stresses in rectangular composite laminates, *Composite Structures*, 27, 419-439, 1994.

[10] S. Brischetto and E. Carrera, Heat conduction and thermal analysis in multilayered plates and shells, *Mechanics Research Communications*, 38, 449-455, 2011.

[11] S. Brischetto, Effect of the through-the-thickness temperature distribution on the response of layered and composite shells, *International Journal of Applied Mechanics*, 1, 581-605, 2009.

[12] S. Brischetto and E. Carrera, Thermal stress analysis by refined multilayered composite shell theories, *Journal of Thermal Stresses*, 32, 165-186, 2009.

[13] S.H. Lo, Wu Zhen, Y.K. Cheung and Chen Wanji, Hygrothermal effects on multilayered composite plates using a refined higher order theory, *Composite Structures*, 92, 633-646, 2010.

[14] N.V.S. Naidu and P.K. Sinha, Nonlinear finite element analysis of laminated composite shells in hygrothermal environments, *Composite Structures*, 69, 387-395, 2005.

[15] C. Wüthrich, Thick-walled composite tubes under mechanical and hygrothermal loading, *Composites*, 23, 407-413, 1992.

[16] G.A. Kardomateas and C.B. Chung, Boundary layer transient hygroscopic stresses in orthotropic thick shells under external pressure, *Journal of Applied Mechanics*, 61, 161-168, 1994.

[17] L.P. Kollár and J.M. Patterson, Composite cylindrical segments subjected to hygrothermal and mechanical loads, *International Journal of Solids and Structures*, 30, 2525-2545, 1993.

[18] S. Kumari and P.K. Sinha, Hygrothermal analysis of composite wing T-joints, *Aircraft Engineering and Aerospace Technology*, 74, 23-37, 2002.

[19] A. Lal, B.N. Singh and S. Anand, Nonlinear bending response of laminated composite spherical shell panel with system randomness subjected to hygro-thermo-mechanical loading, *International Journal of Mechanical Sciences*, 53, 855-866, 2011.

[20] A. Nosier and A.K. Miri, Boundary-layer hygrothermal stresses in laminated, composite, circular, cylindrical shell panels, *Archive of Applied Mechanics*, 80, 413-440, 2010.

[21] O. Sayman, Analysis of multi-layered composite cylinders under hygrothermal loading, *Composites: Part A*, 36, 923-933, 2005.

[22] Z. Yifeng and W. Yu, A variational asymptotic approach for hygrothermal analysis of composite laminates, *Composite Structures*, 93, 3229-3238, 2011.

[23] Z. Youssef, F. Jacquemin, D. Gloaguen and R. Guillén A multi-scale analysis of composite structures: application to the design of accelerated hygrothermal cycles, *Composite Structures*, 82, 302-309, 2008.

[24] A. Ghosh, Hygrothermal effects on the initiation and propagation of damage in composite shells, *Aircraft Engineering and Aerospace Technology: An International Journal*, 4, 386-399, 2008.

[25] P.K. Parhi, S.K. Bhattacharyya and P.K. Sinha, Hygrothermal effects on the dynamic behavior of multiple delaminated composite plates and shells, *Journal of Sound and Vibration*, 248, 195-214, 2001.

[26] H.K. Cho, Optimization of dynamic behaviors of an orthotropic composite shell subjected to hygrothermal environment, *Finite Elements in Analysis and Design*, 45, 852-860, 2009.

[27] Z. Mecitoğlu and H. Örenel, Dynamic behavior of a stiffened laminated conical shell under hygrothermal loads, *Mathematical and Computational Applications*, 1, 73-84, 1996.

[28] S. Raja, P.K. Sinha, G. Prathap and D. Dwarakanathan, Influence of active stiffening on dynamic behaviour of piezo-hygro-thermo-elastic composite plates and shells, *Journal of Sound and Vibration*, 278, 257-283, 2004.

[29] C.K. Kundu and J.-H. Han, Vibration characteristics and snapping behavior of hygro-thermo-elastic composite doubly curved shells, *Composite Structures*, 91, 306-317, 2009.

[30] H.-S. Shen, The effects of hygrothermal conditions on the postbuckling of shear deformable laminated cylindrical shells, *International Journal of Solids and Structures*, 38, 6357-6380, 2001.

[31] N.N. Huang, Viscoelastic buckling and postbuckling of circular cylindrical laminated shells in hygrothermal environment, *Journal of Marine Science and Technology*, 2, 9-16, 1994.

[32] C.H. Kundu and J.-H. Han, Nonlinear buckling analysis of hygrothermoelastic composite shell panels using finite element method, *Composites: Part B*, 40, 313-328, 2009.

[33] A. Lal, B.N. Singh and S. Kale, Stochastic post buckling analysis of laminated composite cylindrical shell panel subjected to hygrothermomechanical loading, *Composite Structures*, 93, 1187-1200, 2011.

[34] H.-S. Shen, Hygrothermal effects on the postbuckling of axially loaded shear deformable laminated cylindrical panels, *Composite Structures*, 56, 73-85, 2002.

[35] H.-S. Shen, Hygrothermal effects on the postbuckling of composite laminated cylindrical shells, *Composites Science and Technology*, 60, 1227-1240, 2000.

[36] X. Wang and H.L. Dai, Non-linear solution for locally delaminated buckling near the surface of a laminated cylindrical shell under hydrothermal environment, *International Journal of Pressure Vessels and Piping*, 80, 243-251, 2003.

[37] X. Wang, Y.C. Zhang and H.L. Dai, Critical strain for a locally elliptical delamination near the surface of a cylindrical laminated shell under hydrothermal effects, *Composite Structures*, 67, 491-499, 2005.

[38] E. Carrera, S. Brischetto and P. Nali, *Plates and Shells for Smart Structures. Classical and Advanced Theories for Modeling and Analysis*, John Wiley & Sons, Ltd, New Delhi, India, 2011.

[39] J.G. Ren, Exact solutions for laminated cylindrical shells in cylindrical bending, *Composite Science and Technology*, 29, 169-187, 1987.

[40] R.K. Khare, T. Kant and A.K. Garg, Closed-form thermo-mechanical solutions of higher-order theories of cross-ply laminated shallow shells, *Composite Structures*, 59, 313-340, 2003.

[41] A.W. Leissa, *Vibration of Shells*, NASA SP-288, Washington, D.C. (USA), 1973.

	$\bar{w}(0)$	$\bar{\sigma}_{\alpha\alpha}(h/2)$	$\bar{\sigma}_{\beta\beta}(h/2)$	$\bar{\sigma}_{\alpha z}(h/4)$
		$R_\alpha/h = 10$		
$3D[39]$	0.493	2.245	0.0250	0.879
CLT	0.445	2.246	0.0225	0.560
$FSDT$	0.488	2.246	0.0225	0.560
$ED4$	0.496	2.266	0.0245	0.797
$LD4$	0.493	2.245	0.0249	0.881
		$R_\alpha/h = 500$		
$3D[39]$	0.399	2.153	0.0215	0.865
CLT	0.399	2.153	0.0215	0.536
$FSDT$	0.399	2.153	0.0215	0.536
$ED4$	0.399	2.153	0.0211	0.769
$LD4$	0.399	2.153	0.0215	0.865

Table 1: First assessment, two-layered composite cylindrical shell subjected to a transverse mechanical pressure, normalized maximum stresses and deflections.

	$\bar{w}$		
R_β/h	50	100	500
$HOST12[40](\theta_a = +0.5K, -0.5K)$	1.0224	1.0299	1.0325
$LD4(\theta_a = +0.5K, -0.5K)$	1.0207	1.0283	1.0306
$LD4(\theta_c = +0.5K, -0.5K)$	0.9643	0.9715	0.9737
$LD2(\theta_a = +0.5K, -0.5K)$	1.0207	1.0283	1.0306
$LD2(\theta_c = +0.5K, -0.5K)$	0.9613	0.9684	0.9706
$ED4(\theta_a = +0.5K, -0.5K)$	1.0208	1.0279	1.0301
$ED4(\theta_c = +0.5K, -0.5K)$	0.9642	0.9709	0.9730
$ED3(\theta_a = +0.5K, -0.5K)$	1.0208	1.0279	1.0301
$ED3(\theta_c = +0.5K, -0.5K)$	0.9640	0.9707	0.9728
$FSDT(\theta_a = +0.5K, -0.5K)$	1.0468	1.0533	1.0551
$FSDT(\theta_c = +0.5K, -0.5K)$	0.9872	0.9933	0.9951
$CLT(\theta_a = +0.5K, -0.5K)$	1.0496	1.0540	1.0552
$CLT(\theta_c = +0.5K, -0.5K)$	0.9898	0.9940	0.9951

Table 2: Second assessment, ten-layered composite cylindrical shell with imposed over-temperature at the external surfaces $\theta_{top} = +0.5K$ and $\theta_{bot} = -0.5K$ which means gradient $\Delta\theta = 1K$.

	$R_\alpha/h = 10$			
	$w[10^{-6}m](h/2)$	$\sigma_{\alpha\alpha}[KPa](h/2)$	$\sigma_{\alpha\beta}[KPa](h/4)$	$\sigma_{\alpha z}[KPa](-h/4)$
$LD4$	0.5970	4.9603	0.1580	0.2212
$ED4$	0.6003	5.1783	0.1859	0.1944
$FSDT$	0.3115	0.5746	-0.0645	0.1600
CLT	0.0421	0.3384	-0.0787	\
$LD4(\theta_a = 50K)$	888.02	-15927	-1101.1	-825.78
$LD4(\theta_a = 50K, 0K)$	765.17	-16343	-916.95	-399.11
$LD4(\theta_c = 50K, 0K)$	538.63	-19633	-641.07	-179.80
$LD4(\mathcal{M}_a = 0.5\%)$	830.25	-14800	-1087.5	-717.78
$LD4(\mathcal{M}_a = 0.5\%, 0.1\%)$	738.17	-15118	-915.79	-445.55
$LD4(\mathcal{M}_c = 0.5\%, 0.1\%)$	582.22	-16817	-696.00	-262.34
$ED4(\mathcal{M}_a = 0.5\%)$	826.22	-15057	-1054.1	-763.60
$ED4(\mathcal{M}_a = 0.5\%, 0.1\%)$	732.35	-15205	-888.63	-472.41
$ED4(\mathcal{M}_c = 0.5\%, 0.1\%)$	572.16	-16181	-673.34	-262.12

Table 3: Displacement and stress evaluation for bending analysis of moderately thick two-layered composite shell in hygrothermal environment.

	$R_\alpha/h = 500$			
	$w[10^{-3}m](h/2)$	$\sigma_{\alpha\alpha}[MPa](h/2)$	$\sigma_{\alpha\beta}[MPa](h/4)$	$\sigma_{\alpha z}[MPa](-h/4)$
$LD4$	0.6936	0.6183	0.3890	-0.0059
$ED4$	0.6936	0.6158	0.3890	-0.0066
$FSDT$	0.6940	0.6151	0.3889	-0.0069
CLT	0.6938	0.6151	0.3888	\
$LD4(\theta_a = 50K)$	0.7630	-17.155	-0.4136	-0.0199
$LD4(\theta_a = 50K, 0K)$	1.3446	-16.912	0.1547	-0.0227
$LD4(\theta_c = 50K, 0K)$	1.3444	-16.916	0.1551	-0.0227
$LD4(\mathcal{M}_a = 0.5\%)$	0.9607	-15.716	-0.3771	-0.0185
$LD4(\mathcal{M}_a = 0.5\%, 0.1\%)$	1.2841	-15.657	0.0647	-0.0214
$LD4(\mathcal{M}_c = 0.5\%, 0.1\%)$	1.2840	-15.658	0.0648	-0.0214
$ED4(\mathcal{M}_a = 0.5\%)$	0.9608	-15.717	-0.3771	-0.0205
$ED4(\mathcal{M}_a = 0.5\%, 0.1\%)$	1.2841	-15.661	0.0647	-0.0230
$ED4(\mathcal{M}_c = 0.5\%, 0.1\%)$	1.2840	-15.661	0.0648	-0.0230

Table 4: Displacement and stress evaluation for bending analysis of thin two-layered composite shell in hygrothermal environment.

	$R_\alpha/h = 10$			
	$w[10^{-6}m](h/2)$	$\sigma_{\alpha\alpha}[KPa](h/2)$	$\sigma_{\alpha\beta}[KPa](h/3)$	$\sigma_{\alpha z}[KPa](-h/3)$
$LD4$	1.3966	25.089	1.1291	0.2250
$ED4$	1.3619	23.627	1.1389	0.4257
$FSDT$	0.5064	7.2916	-0.0096	0.2866
CLT	0.0281	0.8244	-0.0585	\
$LD4(\theta_a = 50K)$	1745.7	30098	-532.78	-458.78
$LD4(\theta_a = 50K, 0K)$	1272.9	21299	-311.78	-199.84
$LD4(\theta_c = 50K, 0K)$	809.54	12642	-117.06	-68.531
$LD4(\mathcal{M}_a = 0.5\%)$	1226.3	17897	-481.23	-200.11
$LD4(\mathcal{M}_a = 0.5\%, 0.1\%)$	1011.9	13814	-343.79	-123.79
$LD4(\mathcal{M}_c = 0.5\%, 0.1\%)$	906.03	11761	-296.61	-84.256
$ED4(\mathcal{M}_a = 0.5\%)$	1289.2	20726	-683.99	-385.73
$ED4(\mathcal{M}_a = 0.5\%, 0.1\%)$	1045.3	15166	-466.78	-292.25
$ED4(\mathcal{M}_c = 0.5\%, 0.1\%)$	928.67	12136	-383.61	-259.18

Table 5: Displacement and stress evaluation for bending analysis of moderately thick five-layered sandwich shell in hygrothermal environment.

	$R_\alpha/h = 500$			
	$w[10^{-3}m](h/2)$	$\sigma_{\alpha\alpha}[MPa](h/2)$	$\sigma_{\alpha\beta}[MPa](h/3)$	$\sigma_{\alpha z}[MPa](-h/3)$
$LD4$	1.1642	14.855	0.5142	-0.0035
$ED4$	1.1621	14.899	0.5138	-0.0036
$FSDT$	1.1615	14.820	0.5119	-0.0001
CLT	1.1587	14.787	0.5104	\
$LD4(\theta_a = 50K)$	3.4916	48.258	-0.2053	-0.0233
$LD4(\theta_a = 50K, 0K)$	2.7942	36.582	0.3585	-0.0181
$LD4(\theta_c = 50K, 0K)$	2.8664	37.503	0.3904	-0.0190
$LD4(\mathcal{M}_a = 0.5\%)$	2.8973	36.163	-0.0228	-0.0148
$LD4(\mathcal{M}_a = 0.5\%, 0.1\%)$	2.5505	30.081	0.3435	-0.0145
$LD4(\mathcal{M}_c = 0.5\%, 0.1\%)$	2.6275	31.065	0.3773	-0.0156
$ED4(\mathcal{M}_a = 0.5\%)$	2.9055	35.823	-0.0280	-0.0181
$ED4(\mathcal{M}_a = 0.5\%, 0.1\%)$	2.5569	29.751	0.3416	-0.0202
$ED4(\mathcal{M}_c = 0.5\%, 0.1\%)$	2.6356	30.451	0.3762	-0.0229

Table 6: Displacement and stress evaluation for bending analysis of thin five-layered sandwich shell in hygrothermal environment.
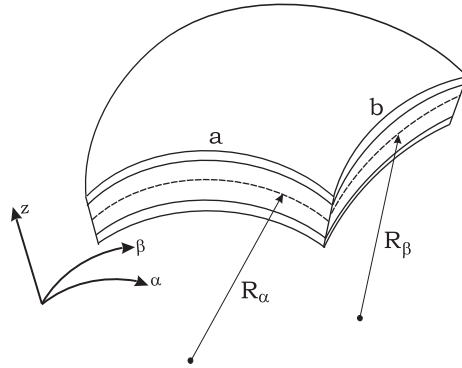
Figure 1: Geometry and reference system for multilayered composite/sandwich spherical shell panels.
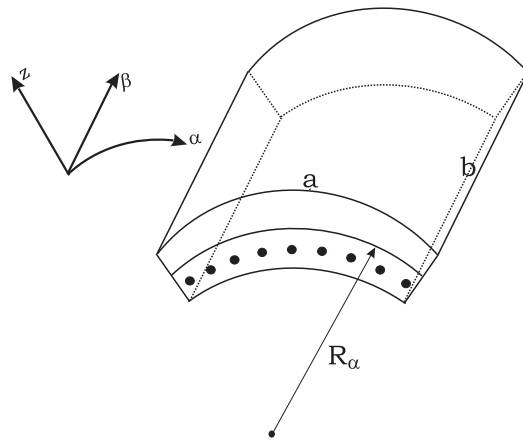

Figure 2: Geometry and reference system for multilayered composite/sandwich cylindrical shell panels.
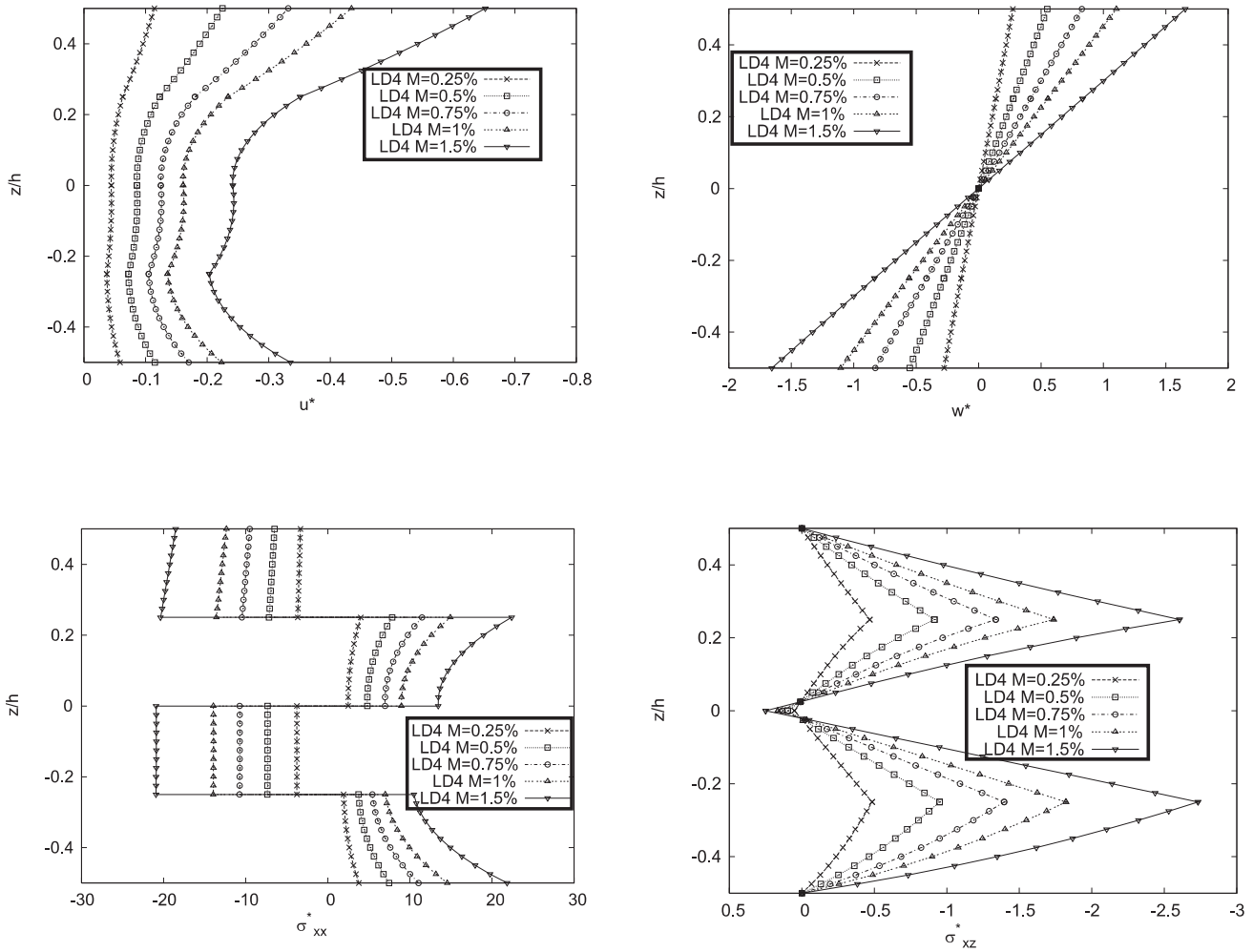
23

Figure 3: Third assessment, constant-through-the-thickness moisture content profile for a four-layered composite plate. LD4 model when the material properties also change with the moisture content.
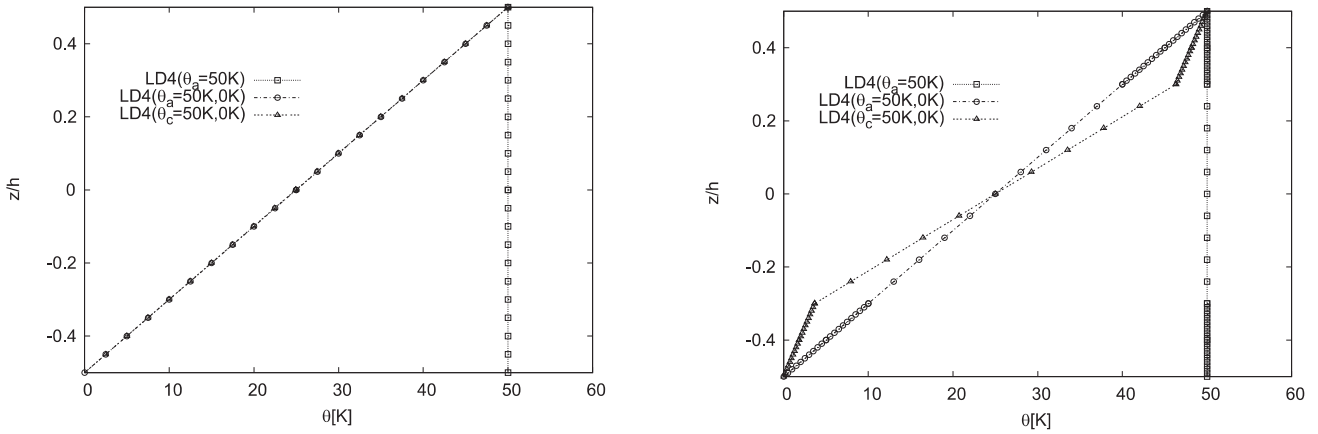

Figure 4: Over-temperature evaluation through the thickness of a thin shell ($R_\alpha/h = 500$). Comparison between assumed constant, assumed linear and calculated temperature profile for the two-layered composite (on the left) and five-layered sandwich (on the right) shell.
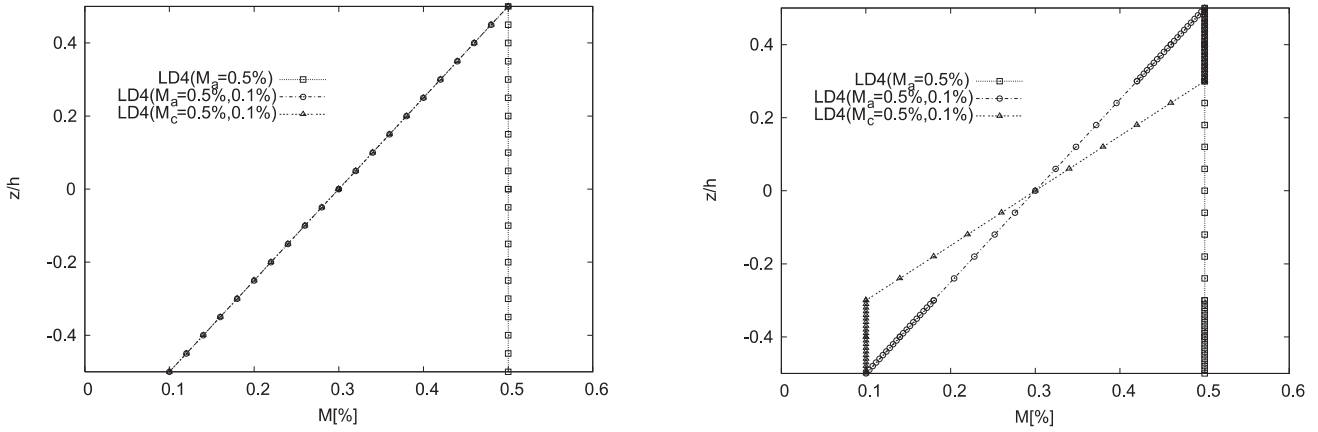
Figure 5: Moisture content evaluation through the thickness of a thin shell ($R_\alpha/h = 500$). Comparison between assumed constant, assumed linear and calculated moisture content profile for the two-layered composite (on the left) and five-layered sandwich (on the right) shell.
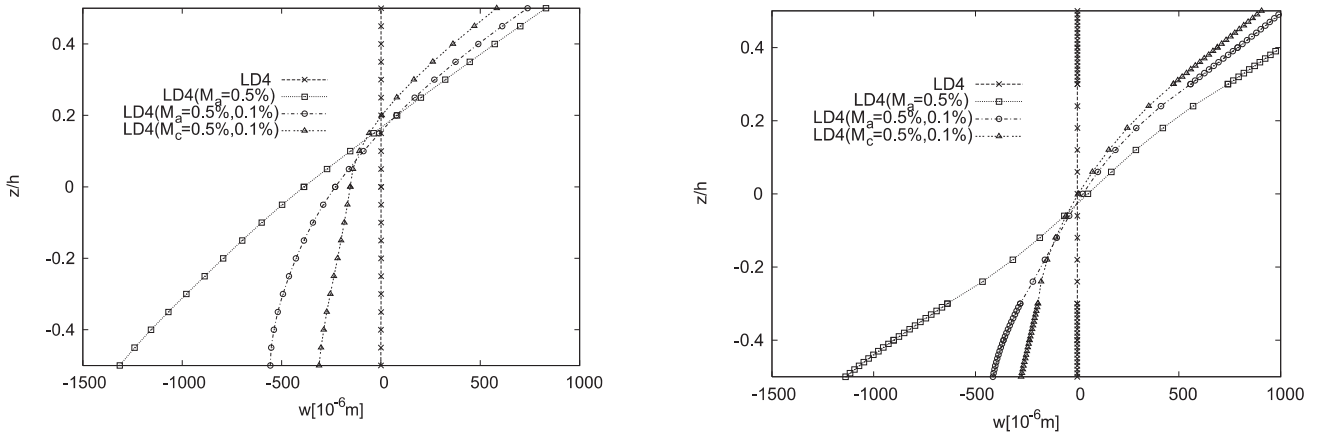

Figure 6: Transverse displacement evaluation through the thickness of a moderately thick shell ($R_\alpha/h = 10$). Comparison between pure mechanical case and different moisture content profiles for the two-layered composite (on the left) and five-layered sandwich (on the right) shell.
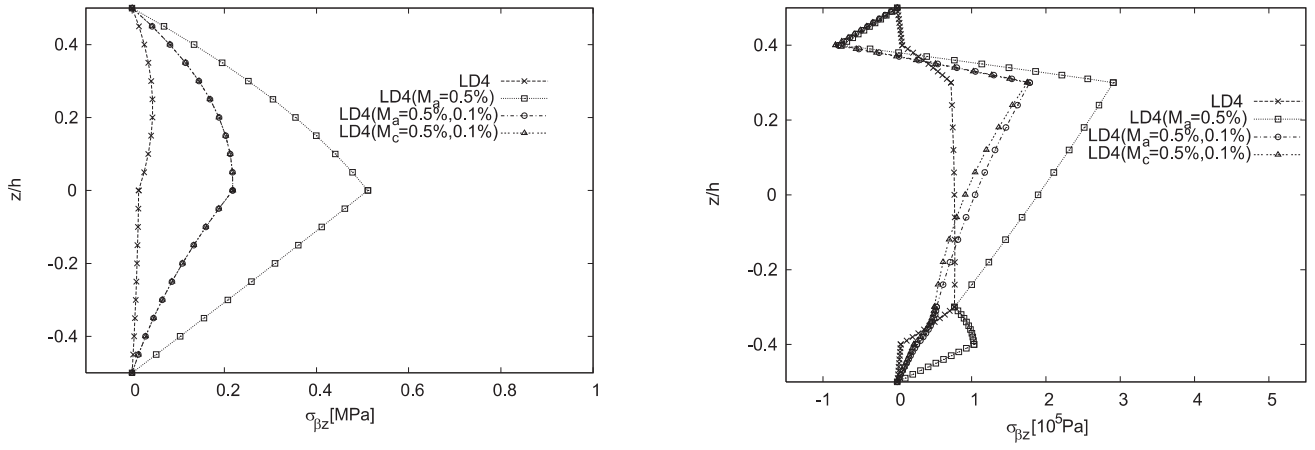
Figure 7: Transverse shear stress evaluation through the thickness of a thin shell ($R_\alpha/h = 500$). Comparison between pure mechanical case and different moisture content profiles for the two-layered composite (on the left) and five-layered sandwich (on the right) shell.